Optimal Design of Multistage Centrifugal Pump Based on the Combined Energy Loss Model and Computational Fluid Dynamics

Chuan Wang [a,b], Weidong Shi [a], Xikun Wang [a,b],
Jiang Xiaoping [a], Yang Yang [a], Wei Li [a] and Ling Zhou [a,*]

[a] *Research Center of Fluid Machinery Engineering and Technology*
Jiangsu University
Zhenjiang, Jiangsu Province
212013, China

[b] *Maritime Research Centre*
Nanyang Technological University
639798, Singapore

[*] Corresponding author.
E-mail address: *lingzhou@ujs.edu.cn*

Abstract: This paper proposes a method to optimize the design of a typical multistage centrifugal pump based on energy loss model and Computational Fluid Dynamics (ELM/CFD). Different grid numbers, turbulence models, convergence precisions, and surface roughness are calculated for a typical multistage centrifugal pump. External characteristic experiments are also conducted to benchmark the numerical simulation. Based on the results, the ELM/CFD method was established including various kinds of energy loss in the pump, such as disk friction loss, volumetric leakage loss, interstage leakage loss as well as the hydraulic loss, which occurred at inlet section, outlet section, impeller, diffuser and pump cavity, respectively. The interactive relationships among the different types of energy losses were systematically assessed. Applying suitable setting methods for numerical calculation renders more credible results, and ensuring the integrity of the calculation model is the key contributor to the accuracy of the results. The interstage leakage loss is converted by the disk friction loss; thus, they are positively correlated, that is, the disk friction loss can be reduced

by decreasing the interstage leakage loss. Concurrently, the volumetric leakage loss is negatively correlated with the disk friction loss; thus, increasing the volumetric leakage loss can effectively reduce the disk friction loss. The increment of the volumetric leakage loss is greater than the decrement of the disk friction loss for general centrifugal pumps. This relationship between these types of losses, however, does not apply to pumps with significantly low specific speed. Therefore, reducing the volumetric leakage and interstage leakage losses is the most effective technique to increase the efficiency of general centrifugal pumps. The impeller should be designed according to the maximum flow design method, because the inevitable volumetric leakage loss will improve the pump efficiency under rated flow condition. Several methods have been proposed to improve the pump efficiency.

Keywords: Energy loss model; Pump optimization; Multistage centrifugal pump; Computational fluid dynamics.

1. Introduction

Pumps are a kind of general machinery with varied applications. According to the statistics, pumps' energy consumption accounts for nearly 22% of the world's energy used by electric motors, so pumps have huge energy consumption and great energy saving potential [1-3]. More and more energy saving strategies and end-users push industries and researchers to concentrate on improving the pump efficiency [4-5]. In addition, multistage centrifugal pumps, as fundamental elements for providing high-energy liquid, have attracted increasing attention in the past several years [6-10].

At present, there are several methods to improve the pump efficiency, namely, test optimization, velocity coefficient optimization, Computational Fluid Dynamics (CFD) optimization and energy loss model (ELM) optimization. Being semi-theoretical and semi-empirical, test optimization plays an important role in the pump design, and orthogonal tests are widely used in the industry. For example, Zhou et al. [11] designed 16 impellers with the same diffuser base on the orthogonal table, and the best parameter combination for the highest pump efficiency was captured by employing the orthogonal tests optimization. In order to improve the efficiency of

stainless steel stamping multistage pump, Wang et al. [12] established the function relationship between the efficiency and three factors of impeller through the quadratic regression orthogonal test. To realize the multiobjective optimization of pump efficiency and cavitation performance, Xu [13] used orthogonal method to carry out the range analysis and studied the influence order of each parameter. Although orthogonal test is very credible and effective for the pump optimization, but it consumes too much time and material because of a series of testing schemes.

Velocity coefficient optimization is a kind of similar conversion method based on lots of excellent hydraulic models, and suitable velocity coefficient should be selected as the basis of pump size according to the specific speed. This method is simple to use, but it's very difficult to design new excellent hydraulic model due to the limitation of existing models and experience. In 1948, Stepanoff [14] presented the Stepanoff velocity diagram by collecting a large number of measured data, using which pump designer can choose the appropriate geometry parameters of the pump according to its specific speed. Lobanof [15] provided the newest velocity coefficient data to calculate the geometric parameters of centrifugal impeller. Yan et al. [16] solved the Lobanof's data through numerical analysis. Although velocity coefficient method is rather effective, but it completely depends on the past empirical coefficients.

Computational Fluid Dynamics (CFD) optimization is to guide the pump optimization through the simulation of the three-dimensional incompressible flow field of the pump by means of high performance computer [17-18]. In recent years, researchers have developed this method firstly on the preliminary design with one-dimensional theory and then CFD optimization. Goto et al. [19] presented the hydraulic design method of centrifugal impeller based on the whole three-dimensional inverse problem design. Passrucker [20] designed inversely the axial plane projection and blade molded line of impeller by using CFD. Zhou et al. [21] simulated the internal flow of a new type of three-dimensional surface return diffuser to improve the hydrodynamic performance of the deep-well centrifugal pump. Although this method is very convenient to optimize the pump efficiency, but it entirely relies on the high-performance computer and experienced technicians using CFD.

The core idea of energy loss model (ELM) optimization is to build the relationships between the geometrical parameters and the various kinds of energy losses in the pump, with an ultimate goal to minimize the total energy loss. The energy losses in the pump are composed of mechanical loss, leakage loss and hydraulic loss. The mechanical loss refers to the energy loss due to the mechanical friction in the pump, including the disk friction loss, bearing friction loss and shaft seal friction loss. The leakage loss refers to the energy loss because of clearance leakage in the pump, including the leakage loss at front ring, rear ring and balance mechanism. The hydraulic loss refers to the energy loss through the various components in the pump, including the inlet section, outlet section, impeller, diffuser and pump cavity. It should be noted that the leakage loss at front ring and rear ring are also called the volumetric leakage loss and the interstage leakage loss, respectively. Due to the complex turbulent flow in the pump, it is very difficult to exactly calculate all the kinds of energy losses in theory, but researchers have deduced many semi-theoretical formulas to estimate the energy losses. For instance, the National Engineering Laboratory of Britain (NELB) applied successfully the ELM optimization in the design of centrifugal pump and mixed-flow pump [22]. Yuan et al. [23] established the predicted ELS of centrifugal pump according to the flow channel centerline method of NELB. Based on the hydraulic loss in the pump, Neumann [24] built the relationship between the geometric parameters and the hydraulic parameters such as flow coefficient, head coefficient and velocity coefficient. Li [25] generalized the Neumann's method to all the blade-pump, and proposed the correction measure for all the blade-pump under the un-design working condition in the principle of minimizing the sum of all the energy losses. Although there are a great number of semi-theoretical formulas for ELM, it is worth asking whether the formulas are accurate or not, either by experimental or numerical methods.

As reviewed above, each of the four optimization methods has its own pros and cons. Test optimization is accurate and reliable, but is time-and resource-consuming. Velocity coefficient optimization is simple and effective, but it is rather difficult to develop new excellent hydraulic model. ELM optimization is based on strict

mathematical theory, but its accuracy is hard to ensure because a lot of internal energy losses are deduced by semi-theoretical formulas. CFD optimization is not restricted by physical model and test apparatus, which saves time and money substantially, but due to the lack of standards for judging whether CFD results are accurate or not, it has to be validated against experimental results. Moreover, most of current numerical calculations can only predict the pump's overall performance, and fall short in detailed analysis of the various kinds of energy losses in the pump.

Therefore, in this paper we propose to combine the ELM optimization and CFD optimization together, namely ELM-CFD. By employing numerical simulations, all the kinds of energy losses in a typical multistage centrifugal pump are calculated to assess their individual or combined effects on the pump performance. The optimal design were obtained by the combining method of ELM-CFD and verified by prototype test. This paper provides certain guidance for the optimization of multistage centrifugal pumps.

2. Setting methods for numerical calculation

CFD is suitable for simulating the internal flow field of rotating machinery. Nevertheless, the numerical settings of CFD should be selected appropriately to ensure the reliability of results. Therefore, a series of numerical calculations for a typical multistage centrifugal pump were performed using different grid numbers, turbulence models, convergence precisions, and surface roughness.

2.1 Hydraulic design of the impeller and diffuser

Impellers and diffusers are the core components of centrifugal pumps. The geometric parameters of impellers and diffusers can be obtained using velocity coefficient method, as shown in Table 1. The inlet angle of positive diffuser blades has a small value of $\alpha_3 = 5°$ to extend the flow channel of the positive diffuser. Reducing the outlet angle of the negative diffuser blade will help obtain a steeper head-flow rate curve, lower maximum shaft power [26-27]. Thus, the outlet angle of the negative diffuser blades was set to 50°. Table 1 shows that the two-dimensional models of the impeller and diffuser can be obtained, as respectively shown in Figures 1 and 2.

Tab. 1 Basic geometric parameters of the pump

Geometric parameter	Value	Geometric parameter	Value
Inlet diameter of the impeller D_1 (mm)	20	Outlet width of the impeller blade b_2 (mm)	3
Hub diameter of the impeller D_{hb} (mm)	33.5	Number of positive diffuser blades Z_p	9
Outlet diameter of the impeller D_2 (mm)	108	Number of negative diffuser blades Z_n	9
Inlet angle of the impeller blade β_1 (°)	40	Inlet diameter of the positive diffuser D_3 (mm)	109
Outlet angle of the impeller blade β_2 (°)	15	Inlet angle of the positive diffuser blade α_3 (°)	5
Wrap angle of the impeller blade θ_w (°)	150	Outlet angle of the negative diffuser blade α_6 (°)	50
Number of the impeller blades Z	8	Rated flow Q_r (m^3/h)	3.3

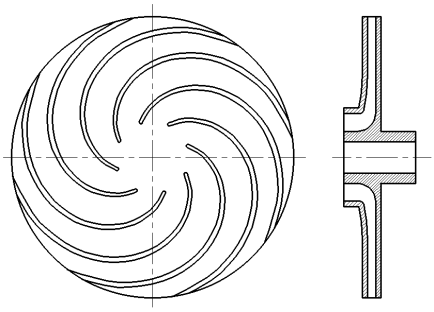

(a) Plane projection (b) Axial projection

Fig. 1 Two-dimensional diagram of the impeller

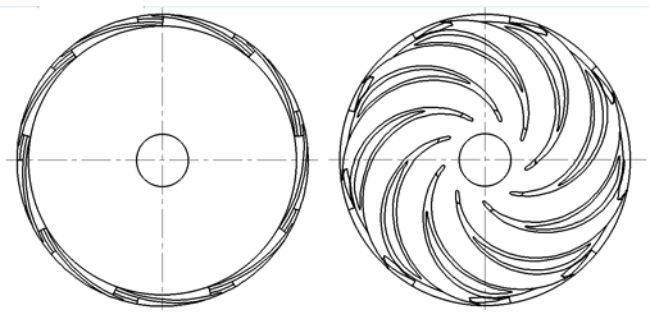

(a) Positive diffuser (b) Negative diffuser

Fig. 2 Two-dimensional diagram of the diffuser

2.2 Establishing the calculation model

The calculation model was the basis for the numerical calculation, and its integrity significantly influenced the numerical results. Four different calculation models were considered to study the various types of energy losses in the pump systematically, as shown in Figure 3.

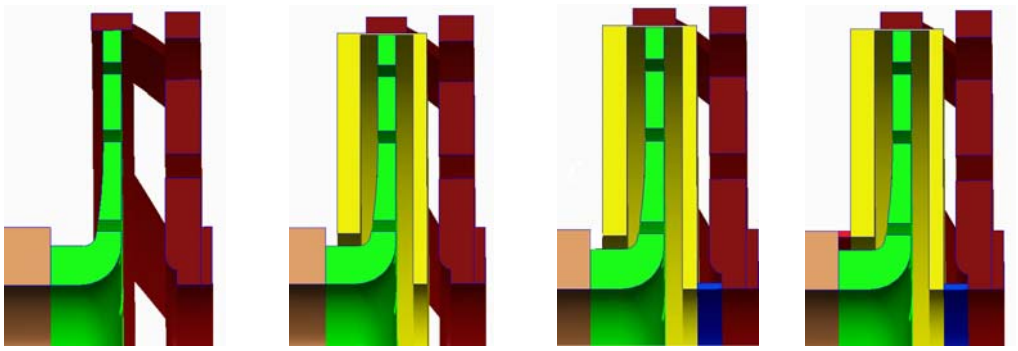

(a) (b) (c) (d)

Fig. 3 Calculation models: (a) Impeller and diffuser; (b) Impeller, diffuser, and pump cavity;

(c) Front or rear ring, impeller, diffuser, and pump cavity; (d) Front and rear rings, impeller, diffuser, and pump cavity.

Only the impeller and diffuser were considered for calculation model (a), ignoring the losses of disk friction and volumetric leakage. Pump cavity was added to calculation model (b), still ignoring volumetric leakage loss was still. A portion of the volumetric leakage loss was disregarded for calculation (c) because only one of the two rings was considered. The entire flow field of the multistage pump was considered in calculation model (d); thus, the numerical result of this model was closer to the actual value than those of the preceding three calculation models.

2.3 Establishing the calculation domain

The stage number of multistage centrifugal pumps depends on user demands. If the flow field of the calculation model with all the stage is simulated, the grid number becomes too large to meet the requirements of a practical engineering application. In addition, multistage centrifugal pumps are more complicated than single-stage centrifugal pumps. The swirling of the inlet flow of the impellers, except for the first one, is caused by the outlet flow of diffusers. The two-stage pump was selected in this study considering the increase of grid number with the increase of the pump stage.

Figure 4 shows that the calculation domain of the two-stage pump includes the inlet section, two impellers, two pump cavities, two diffusers, two front rings, two rear rings, and the outlet section. The lengths of the inlet and outlet sections are respectively five and four times of the diameter of the impeller.

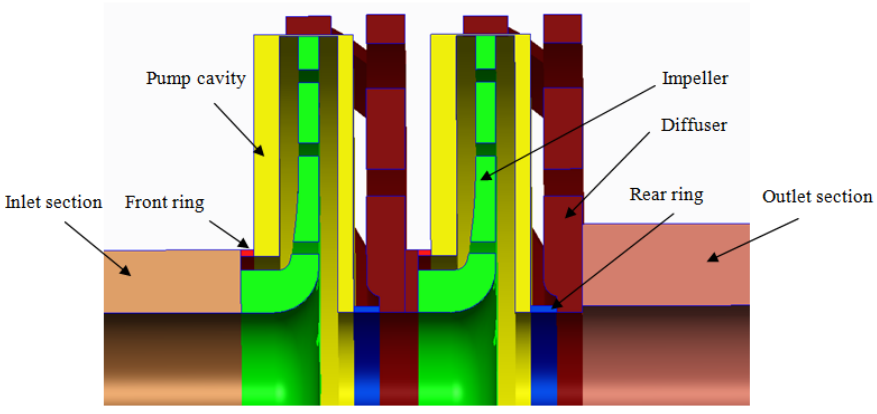

Fig. 4 Calculation domain of the two-stage pump

This analysis suggests that the predicted external characteristics of the multistage pump depend on the parameters of the two-stage pump, which are shown as follows:

$$H = H_{\text{in}} + H_1 + (N-1)H_2 + H_{\text{out}} \tag{1}$$

$$P = P_1 + (N-1)P_2 \tag{2}$$

$$\eta = \frac{\rho g Q H}{P} \tag{3}$$

where H is the total head of the multistage pump (in m); H_{in} is the loss head of the inlet section (in m); H_1 is the head of the first stage (in m); H_2 is the head of the second stage (in m); H_{out} is the loss head of the outlet section (in m); Q is the flow rate (in m^3/h); P, P_1, and P_2 are the shaft power values of the multistage pump, and the first and second stages (in W), respectively; and η is the efficiency of the multistage pump. The calculation results are then translated (through an appropriate procedure) to extrapolate the five-stage pump, for which the experimental data are available and discussed hereinafter.

2.4 Analyzing grid independence

The calculation domain should be discretized before simulation based on grids. In this study, the calculation domain was divided into structured grids by ICEM CFD software. Theoretically, the calculating errors would decrease gradually with an increase in grid number; however, too many grids would pose prohibitive demands on computational resources and time. Five grid sizes (G) with the same numerical settings were selected to determine the appropriate grid number. The results under different flow conditions of Q = 2.64, 3.3 and 3.96 m^3/h are shown in Table 2. Due to that the pump generally works under nearly rated flow condition, so small flow condition and large flow condition are not included herein.

It can be seen that the grid size minimally influences the numerical results, and the overall difference is within 2%. The efficiency η and total head H are slightly high when the grid size is relatively large ($G \geq 1.0$ mm) and are basically stable when $G \leq$ 0.8 mm. G is set to 0.8 mm after considering the computational accuracy and time, and the structured grids of the calculation domain are shown in Figure 5. Of course,

0.8 mm grid size is not a universal principle that can be applied to all scenarios, because the grid size completely depends on the size of the calculation model and the requirement of the grid quality. In principle, grid independence should be made to obtain a suitable gird size for any new calculation models.

Tab. 2 Grid independence test of the pump under different flow conditions

Grid size G (mm)	1.5	1.2	1.0	0.8	0.7
Grid number	1321154	1773142	2399892	3674514	4839030
Nodes	1146888	1537022	2091526	3233200	4289372
Efficiency η of Q = 2.64 m^3/h (%)	40.73	40.12	39.73	39.55	39.51
Efficiency η of Q = 3.3 m^3/h (%)	42.19	41.79	41.43	41.13	41.15
Efficiency η of Q = 3.96 m^3/h (%)	41.64	40.84	40.47	40.26	40.22
Head H of Q = 2.64 m^3/h (m)	48.27	48.04	47.71	47.68	47.64
Head H of Q = 3.3 m^3/h (m)	42.11	41.99	41.62	41.62	41.64
Head H of Q = 3.96 m^3/h (m)	35.68	35.32	35.07	35.02	35.06

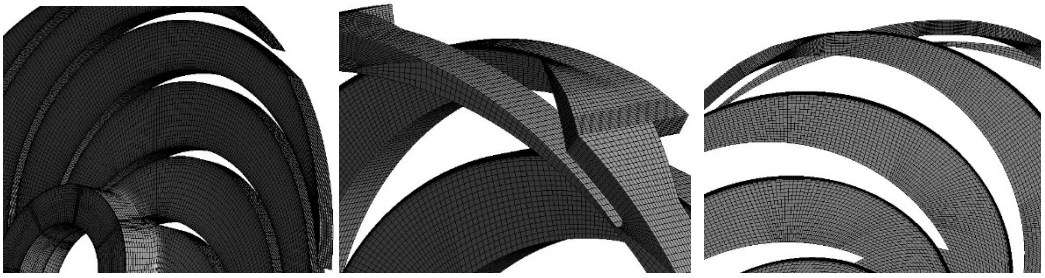

(a) Impeller (b) Positive diffuser (c) Negative diffuser

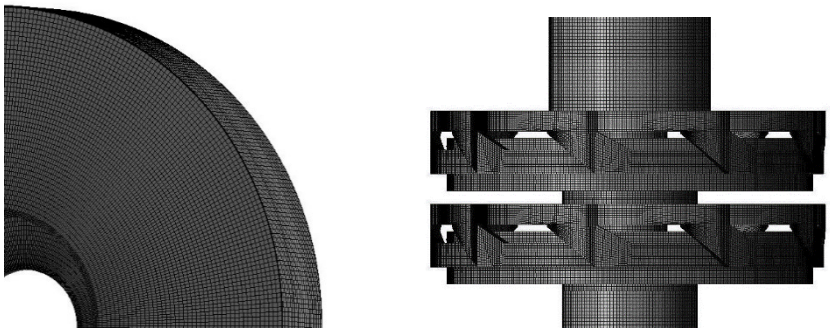

(d) Pump cavity (e) Entire calculation domain

Fig.5 Structured grids of the calculation domain

2.5 Selecting the turbulence model

A universal turbulence model that is applicable for all flow problems has not yet been formulated; thus, scholars have selected different turbulence models for different

turbulent flows. In this study, numerical calculations were performed with ANSYS CFX software, which provides a number of turbulence models. Among the turbulence models, k-ε and k-ω are known to be the most suitable for the internal flow of rotating machines. Therefore, five models, i.e., standard k-ε, RNG k-ε, BSL k-ω, standard k-ω, and SST k-ω, were selected, and their results were compared with the experimental results. Table 3 shows the numerical and experimental results of the pump with different turbulent models under different flow conditions of Q = 2.64, 3.3 and 3.96 m^3/h. It can be found that, after comprehensive comparison, the prediction by standard k-ε model is closest to the experimental data; thus, this model was selected in this study.

Tab. 3 Numerical and experimental results with different turbulent models under different flow conditions

Turbulence model	Standard k-ε	RNG k-ε	BSL k-ω	Standard k-ω	SST k-ω	Test value
Efficiency η of Q = 2.64 m^3/h (%)	39.55	39.84	43.87	43.22	42.53	39.36
Efficiency η of Q = 3.3 m^3/h (%)	41.13	41.28	44.96	44.55	44.59	40.73
Efficiency η of Q = 3.96 m^3/h (%)	40.26	40.49	43.14	42.67	42.15	38.21
Head H of Q = 2.64 m^3/h (m)	47.68	48.04	51.73	51.41	51.56	49.62
Head H of Q = 3.3 m^3/h (m)	41.62	41.12	43.54	43.46	43.50	41.87
Head H of Q = 3.96 m^3/h (m)	35.02	35.41	38.49	38.16	37.72	33.69

2.6 Selecting the convergence precision

Three convergence precisions (10^{-3}, 10^{-4}, and 10^{-5}) were selected to determine a suitable convergence criterion. As shown in Table 4, the numerical results are considerably lower than the experimental results when the convergence precision is 10^{-3}. By contrast, the numerical results tend to be stable when the convergence precision is lower than 10^{-4}. Therefore, 10^{-5} was selected as the value of convergence precision in this study.

Tab. 4 Numerical and experimental results with three convergence precisions under different flow conditions

Convergence precision	10^{-3}	10^{-4}	10^{-5}	Test value
Efficiency η of Q = 2.64 m^3/h (%)	35.43	39.42	39.55	39.36

Efficiency η of Q = 3.3 m^3/h (%)	37.21	41.02	41.13	40.73
Efficiency η of Q = 3.96 m^3/h (%)	34.29	40.19	40.26	38.21
Head H of Q = 2.64 m^3/h (m)	46.87	47.61	47.68	49.62
Head H of Q = 3.3 m^3/h (m)	40.62	41.60	41.62	41.87
Head H of Q = 3.96 m^3/h (m)	32.82	35.09	35.02	33.69

2.7 Influence of surface roughness on the pump performance

Different values of surface roughness (μ = 0, 1, 10, 20, 40, 80 μm) were selected for the numerical calculation of the pump to study the influence of surface roughness on the performance of the pump. The results under different flow conditions are presented in Table 5, wherein H and η continue to decrease with an increase in μ; however, the decrease rate of η is significantly greater than that of H, indicating that the pump shaft power is also increasing. In addition, η and H decreases quickly when μ is low, but their reduction decelerates with the increase of μ. When μ increases from 0 μm to 80 μm for the pump under rated flow condition of Q = 3.3 m^3/h, η decreases from 41.67% to 28.96%, and H decreases from 41.83 m to 35.91 m, with their amplitudes decreasing by 31.06% and 14.19%, respectively. These results demonstrate the significant influence of surface roughness on the numerical results. Therefore, suitable surface roughness should be selected according to the material properties in CFD; otherwise, significant deviations may occur. In this study, the pump was made of polyphenol oxidase and stainless steel, and the value of μ was usually within 1 μm. Therefore, 1 μm was finally selected as the value of surface roughness in the present study. Actually, the surface roughness has significant influence on the numerical results, which was generally underestimated in the past. Sometimes, the value of surface roughness is only selected according to the annotation of the 2D processing chart by many researchers, which might deviates significantly from the actual values of the real machining parts. Therefore, suitable surface roughness should be selected according to the material properties in CFD; otherwise, significant deviations may occur.

Tab. 5 Efficiency and head of the pump with different surface roughness under different flow conditions

Roughness μ (μm)	0	1	10	20	40	80	Test value
Efficiency η of Q = 2.64 m^3/h (%)	40.04	39.55	36.13	34.01	31.74	28.28	39.36
Efficiency η of Q = 3.3 m^3/h (%)	41.67	41.13	37.71	35.34	32.46	28.96	40.73
Efficiency η of Q = 3.96 m^3/h (%)	40.86	40.26	35.82	33.63	30.38	26.22	38.21
Head H of Q = 2.64 m^3/h (m)	47.88	47.68	46.41	45.49	44.46	42.58	49.62
Head H of Q = 3.3 m^3/h (m)	41.83	41.62	40.27	39.25	37.83	35.91	41.87
Head H of Q = 3.96 m^3/h (m)	35.28	35.02	33.44	32.27	30.43	28.26	33.69

2.8 Setting of boundary conditions

The impeller and shroud in the pump chamber were based on the rotating reference frame, whereas the other sub-domains were based on the stationary reference frame throughout the entire calculation domains. The interfaces between the impeller and its adjacent sub-domains were set to "Frozen Rotor" mode, and the other interfaces were set to "General Connection" mode. Moreover, the non-slip walls were selected as the wall boundaries. The open inlet and mass outflow were selected as the inlet and outlet boundaries.

2.9 Comparison between the numerical and experimental results

All field numerical calculations for the two-stage pump were performed with 0.8 mm grid size, Standard k-ε turbulence model, 10^{-5} convergence precision, and 1 μm surface roughness based on the above research. The simulations were performed at five flow points (Q = 1.65, 2.64, 3.3, 3.96, 5.4 m^3/h). At the same time, the hydraulic models were shown to a pump company in Fujian Province, and a five-stage centrifugal pump was manufactured. Then, the pump was sent to the Mechanical Products Testing Center of the Fujian Academy of Mechanical Sciences for performance testing. As shown in Figure 6, the test rig is an open-type system, which is composed of two parts—acquisition and water circulation systems. A turbine flowmeter was used to measure the flow rate Q with a precision of ±0.3%. The pump speed n was measured by a tachometer (PROVA RM-1500, Taiwan) with a precision of ±0.04%. During the experiment, two pressure transmitters (CYG1401, China) with a precision of ±0.2% were used to measure the inlet and outlet pressures.

The comparisons between the numerical and experimental results are presented

in Figure 7. Generally, the predicted H and η are in good agreement with the experimental results at different flow conditions, and they nearly coincide under a rated flow condition of Q=3.3 m^3/h. Some discrepancies exist between the numerical and experimental results because of the flow separation or recirculation in the pump under the non-rated flow conditions, but the deviations are still within 3%. The results show that the performances of the multistage centrifugal pump can be credibly predicted using CFD through the entire calculation model and appropriate numerical setting method.

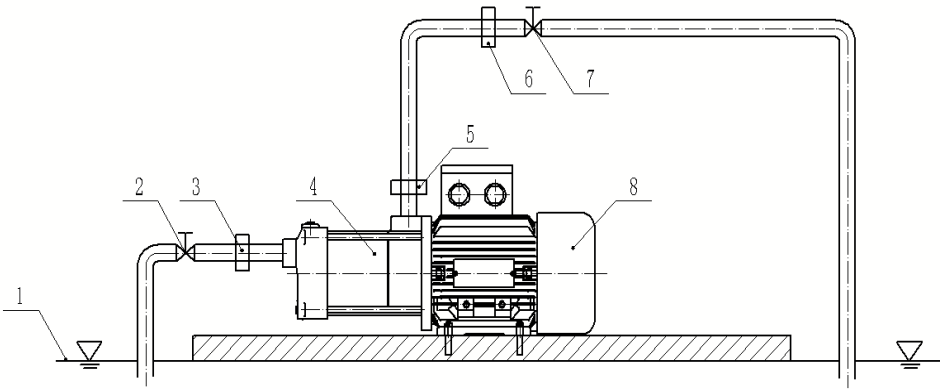

1. Pool 2. Inlet control valve 3. Inlet pressure transmitter 4. Pump 5. Outlet pressure transmitters 6. Turbine flowmeter 7. Flow control valve 8. Motor

Fig. 6 Schematic diagram of the test rig

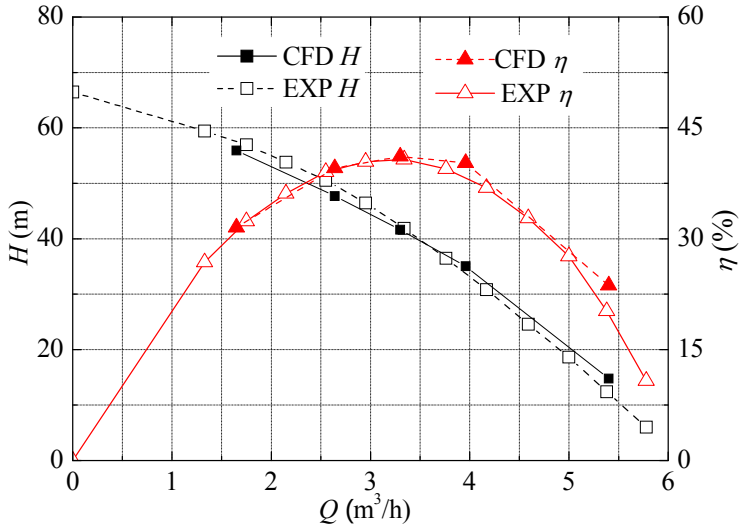

Fig. 7 Numerical and experimental results of the head (H) and efficiency (η) of the pump in relation to roughness (Q)

3. CFD-based assessment of energy losses

3.1 Concept formulas of energy loss model

Based on the foregoing study of numerical setting methods, a loss model method was established to determine the relationships among the different types of energy losses in a multistage centrifugal pump.

First, the efficiency of the multistage pump was divided into three types of component efficiencies. With the mechanical friction loss disregarded, the formulas for component efficiency are as follows:

$$P = P_{\mathrm{m}} + P_{\mathrm{h}} \tag{4}$$

$$P_{\mathrm{m}} = P_{1\mathrm{m}} + (N-1)P_{2\mathrm{m}} \tag{5}$$

$$P_{\mathrm{h}} = P_{1\mathrm{h}} + (N-1)P_{2\mathrm{h}} \tag{6}$$

$$q = \frac{q_1 + (N-1)q_2}{N} \tag{7}$$

$$\eta_{\mathrm{m}} = 1 - \frac{P_{\mathrm{m}}}{P} \tag{8}$$

$$\eta_{\mathrm{v}} = \frac{Q}{Q+q} \tag{9}$$

$$\eta_{\mathrm{h}} = \frac{\eta}{\eta_{\mathrm{m}}\eta_{\mathrm{v}}} \tag{10}$$

where P is the shaft power of the multistage pump (in W), P_{m} is the loss of disk friction power of the multistage pump (in W), P_{h} is the hydraulic power of the multistage pump (in W), $P_{1\mathrm{m}}$ is the loss of disk friction power at the first stage pump (in W), $P_{2\mathrm{m}}$ is the loss of disk friction power at the second stage pump (in W), $P_{1\mathrm{h}}$ is the hydraulic power of the second-stage pump (in W), $P_{2\mathrm{h}}$ is the hydraulic power of the second-stage pump (in W), q is the average ring leakage amount of the multistage pump (in m^3/h), q_1 is the ring leakage amount of the first-stage pump (in m^3/h), q_2 is the ring leakage amount of the second-stage pump (in m^3/h), η_{m} is mechanical efficiency, η_{v} is volumetric efficiency, and η_{h} is hydraulic efficiency.

Second, the total shaft power of the multistage pump was divided into several energy losses, which is as follows:

$$P_{\mathrm{h}} = P_{\mathrm{v}} + P_{\mathrm{u}} + \Delta P_{\mathrm{h}} = \rho g(Q+q)H_{\mathrm{t}} \tag{11}$$

$$P_{\mathrm{v}} = \rho g q H_{\mathrm{t}} = \rho g q(H+h) \tag{12}$$

$$P_{\mathrm{u}} = \rho g Q H \tag{13}$$

$$\Delta P_h = \rho g Q h \tag{14}$$

$$h = H_{\mathrm{in}} + h_{\mathrm{ip}} + h_{\mathrm{df}} + h_{\mathrm{ca}} + H_{\mathrm{out}} \tag{15}$$

Substituting Equation (15) into Equation (14) yields:

$$\Delta P_h = \rho g Q(H_{\mathrm{in}} + h_{\mathrm{ip}} + h_{\mathrm{df}} + h_{\mathrm{ca}} + H_{\mathrm{out}}) = \Delta P_{\mathrm{in}} + \Delta P_{\mathrm{ip}} + \Delta P_{\mathrm{df}} + \Delta P_{\mathrm{ca}} + \Delta P_{\mathrm{out}} \tag{16}$$

Then, substituting Equations (11) and (16) into Equation (4) yields:

$$P = P_{\mathrm{m}} + P_{\mathrm{v}} + P_{\mathrm{u}} + \Delta P_{\mathrm{in}} + \Delta P_{\mathrm{ip}} + \Delta P_{\mathrm{df}} + \Delta P_{\mathrm{ca}} + \Delta P_{\mathrm{out}} \tag{17}$$

where P_{v} is loss of volumetric leakage power (in W), P_{u} is working power (in W), ΔP_{h} is hydraulic loss power (in W), ΔP_{in} is the hydraulic loss power of the inlet section (in W), ΔP_{ip} is the hydraulic loss power of the impeller (in W), ΔP_{df} is the hydraulic loss power of the diffuser (in W), ΔP_{ca} is the hydraulic loss power of the pump cavity (in W), ΔP_{out} is the hydraulic loss power of the outlet section (in W), H_{t} is the theoretical head of the multistage pump (in m), h is the hydraulic loss head of the unit fluid through the pump (in m), h_{ip} is the hydraulic loss head of the unit fluid through the impeller (in m), h_{df} is the hydraulic loss head of the unit fluid through the diffuser (in m), and h_{ca} is the hydraulic loss head of unit of the unit fluid through the pump cavity (in m).

3.2 Performance comparison of different calculation models under rated flow condition

Figure 3 shows that the four calculation models (i.e., without pump cavity, without front ring or rear ring, without front ring, and with 1 mm front ring) gradually considered the losses of hydraulic, friction disk, and interstage leakage at the rear ring, and the volumetric leakage loss at the front ring. The four models were denoted by *M*1, *M*2, *M*3, and *M*6, and two additional models, one with 0.25 mm front ring and the other with 0.5 mm front ring, were denoted by *M*4 and *M*5,

respectively. The numerical results under rated flow condition are shown in Table 6 and Table 7.

Tab. 6 Pump performance in the different calculation models under rated flow condition

Type	M	H (m)	P (W)	q (m^3/h)	η_m (%)	η_v (%)	η_h (%)	η (%)
Without pump cavity	1	50.97	707.04	0	100	100	64.76	64.76
Without ring	2	53.29	875.96	0	79.40	100	68.83	54.65
Without front ring	3	50.21	919.39	0	75.48	100	64.90	49.06
With 0.25 mm front ring	4	45.46	921.57	0.455	78.34	87.89	64.36	44.32
With 0.5 mm front ring	5	43.63	915.91	0.534	79.05	86.07	62.90	42.79
With 1 mm front ring	6	41.62	909.12	0.687	79.15	82.78	62.77	41.13

Tab. 7 Components of the shaft power for different calculation models under rated flow condition

M	P_m (W)	P_v (W)	P_u (W)	ΔP_{in} (W)	ΔP_{ip} (W)	ΔP_{df} (W)	ΔP_{ca} (W)	ΔP_{out} (W)
1	0	0	457.85	0.023	63.12	184.68	0	1.37
2	180.45	0	478.74	0.022	54.65	149.12	11.67	1.30
3	225.45	0	451.05	0.024	50.34	164.94	25.87	1.71
4	199.59	87.41	408.41	0.25	52.02	158.70	13.39	1.79
5	191.88	114.54	383.37	0.14	57.73	156.22	10.24	1.79
6	189.55	123.93	373.89	0.058	59.86	154.99	5.07	1.76

Figure 8 shows the head and efficiency values for different calculation models under rated flow condition. With increasing integrity of the calculation model, the efficiency constantly decreases, and the largest deviation is greater than 23%, whereas the head initially increases and subsequently decreases. The pump head is increased by the rotating disk of *M*2 in the pump and is significantly decreased by the interstage and ring leakages of *M*3, *M*4, *M*5, and *M*6. The largest head difference is approximately 12 m (or about 30%), indicating that the integrity of the calculation model is the key contributor to the accuracy of the results.

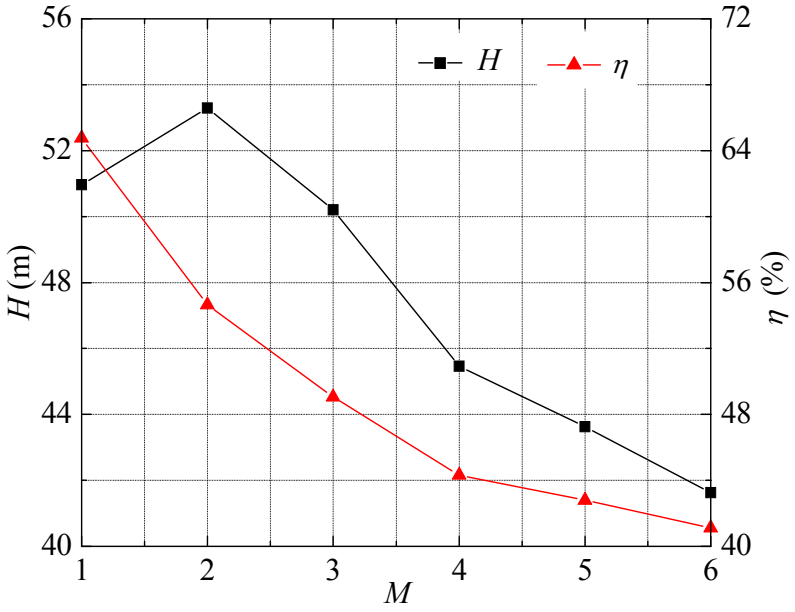

Fig. 8 Head and efficiency values of the different calculation models

Figure 9 presents the mechanical efficiency η_m, hydraulic efficiency η_h, and volumetric efficiency η_v for different calculation models under rated flow condition. As shown in Figure 9 and Table 6, η_v is equal to 100% in the first three models (M = 1, 2, 3), in which the front ring leakage is disregarded. As the clearance of the front ring increases, η_v reduces constantly, but the reduction rate decelerates gradually. This result is attributed to the significant reduction in the pump head rapidly reducing the pressure difference between the two sides of the front ring, leading to the growth rate deceleration of the front ring leakage. For $M2$, η_m decreases by 20% by considering the disk friction loss, whereas it continues to decrease by 4% for $M3$ by considering the interstage leakage loss. This result indicates that a certain portion of the interstage leakage loss is reversed by the disk friction loss. For $M4$, in which the front ring leakage is considered, η_m increases by 3% instead, suggesting that the volumetric leakage can actually decrease disk friction loss. As the clearance of the front ring increases (from $M5$ to $M6$), η_m continues to increase, but the increase rate reduces significantly. Moreover, η_h increases by 4% for $M2$ by considering the disk friction loss, which is ascribed to the increasing head by the rotational disk. By contrast, η_h decreases by 4% again for $M3$ by considering the interstage leakage loss, indicating that the remaining interstage leakage loss is also converted by the disk friction loss. After the front ring leakage is considered, η_h decreases, and the reduction rate

decelerates gradually because the actual flow through the impeller is enhanced, and the operation point shifts to the large flow direction.

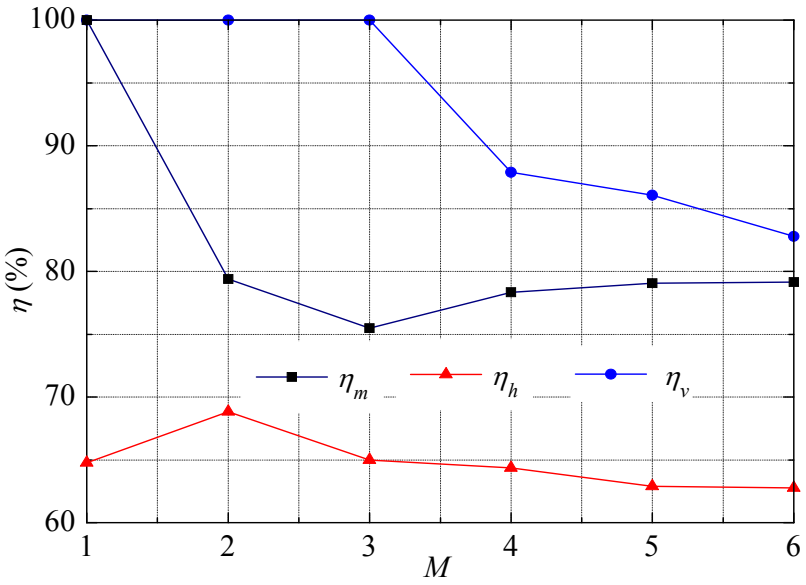

Fig. 9 Mechanical, hydraulic, and volumetric efficiencies of the different calculation models

Figure 10 shows the components of the shaft power of the pump for different calculation models under rated flow condition. The hydraulic loss powers of the inlet and outlet sections are negligible; thus, they are not included in Figure 10. The shaft power is minimal for *M*1 because only the hydraulic losses power of the impeller and diffuser are considered. The losses of disk friction and working powers increase significantly for *M*2 by considering the flow in the pump cavity. The losses of disk friction and hydraulic powers increase for *M*3 by considering the interstage leakage. The loss of volumetric power increases significantly, and that of the disk friction power decreases obviously for *M*4 by considering the front ring leakage. With an increase in the clearance of the front ring, the loss of volumetric power continues to increase, and that of the disk friction power continues to decrease for *M*5 and *M*6; however, their change rate gradually decelerates. Using the components of the shaft power of the pump for *M*6 as an example, the losses of disk friction, hydraulic, and volumetric powers of the diffuser account for 21%, 17%, and 13%, respectively, whereas the working power of the pump only accounts for 40%. These results support the premise that reducing the proportion of these three types of energy losses increases pump efficiency. The loss of disk friction power has a significant negative

correlation with that of the volumetric power; thus, reducing the hydraulic loss power of the diffuser is an effective method to increase the efficiency of the centrifugal pump with low specific speed. Previous scholars, however, paid more attention to the hydraulic improvement of the impeller.

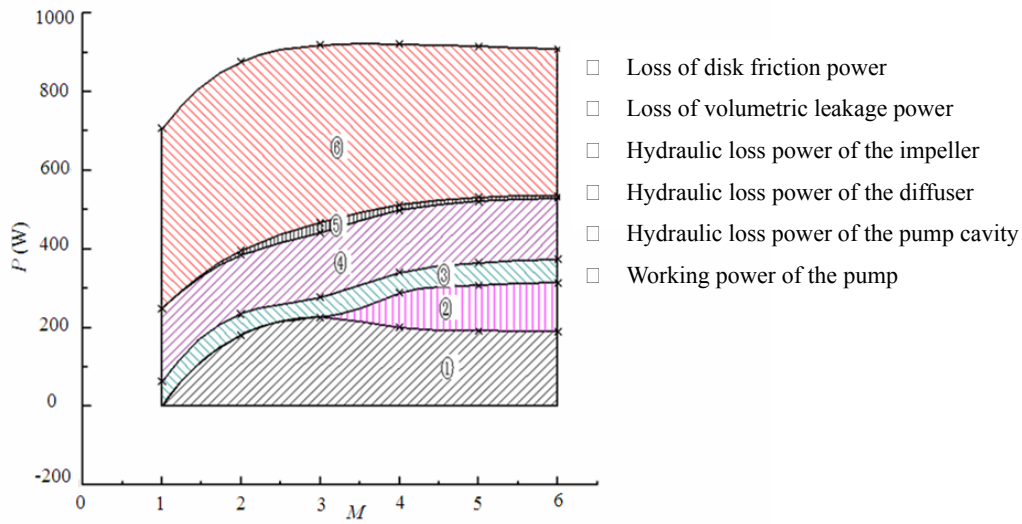

Fig. 10 Components of the shaft power of the different calculation models

3.3 Performance comparison of three typical calculation models under different flow conditions

*M*2, *M*3, and *M*6 were selected for case studies to further investigate the interaction relationships among the three sub-efficiencies. These three calculation models successively considered the losses of disk friction, interstage leakage at the rear ring, and volumetric leakage at the front ring, whereas the clearances of the front and rear rings were set to 1 mm. The performances of the three calculation models under different flow conditions are shown in Tables 8 and 9.

Tab. 8 Pump's performances in the three models under different flow conditions

Q (m^3/h)	M	H (m)	P (W)	q (m^3/h)	q_b(m^3/h)*	η_m (%)	η_v (%)	η_h (%)	η (%)
1.65	2	69.22	744.20	0	0	73.66	100	56.72	41.78
2.64	2	60.03	817.67	0	0	77.24	100	68.31	52.76
3.3	2	53.29	875.96	0	0	79.40	100	68.83	54.65
3.96	2	45.63	934.27	0	0	80.79	100	65.17	52.65
5.4	2	21.91	969.65	0	0	81.40	100	40.27	32.78
1.65	3	67.09	776.03	0	0.247	68.09	100	57.03	38.83
2.64	3	56.87	859.27	0	0.210	72.70	100	65.43	47.56
3.3	3	50.21	919.39	0	0.178	75.48	100	65.00	49.06
3.96	3	42.91	967.50	0	0.134	77.78	100	61.48	47.81

5.4	3	21.45	971.34	0	0.00602	81.27	100	39.94	32.46
1.65	6	55.92	796.63	0.877	0.224	73.83	65.29	65.71	31.53
2.64	6	47.68	866.52	0.752	0.190	77.33	77.83	65.88	39.55
3.3	6	41.62	909.12	0.687	0.156	79.15	82.78	62.77	41.13
3.96	6	35.02	937.65	0.636	0.114	80.62	86.15	57.97	40.26
5.4	6	14.78	917.09	0.479	0.00351	82.57	91.86	31.25	23.70

* q_b is interstage leakage.

Tab. 9 Components of the shaft power in the three models under different flow conditions

Q (m^3/h)	M	P_m (W)	P_v (W)	P_u (W)	ΔP_{in} (W)	ΔP_{ip} (W)	ΔP_{df} (W)	ΔP_{ca} (W)	ΔP_{out} (W)
1.65	2	196.00	0	310.91	0.0093	93.77	117.80	25.30	0.39
2.64	2	186.07	0	431.46	0.0097	55.48	127.11	16.73	0.83
3.3	2	180.45	0	478.74	0.022	54.65	149.12	11.67	1.30
3.96	2	179.50	0	491.86	0.038	64.37	189.44	6.90	2.16
5.4	2	180.32	0	317.87	0.078	110.35	356.29	0.033	4.71
1.65	3	247.61	0	301.36	0.0022	74.21	86.83	65.54	0.47
2.64	3	234.62	0	408.68	0.012	47.43	129.16	38.26	1.12
3.3	3	225.45	0	451.05	0.024	50.34	164.94	25.87	1.71
3.96	3	215.02	0	462.59	0.039	62.29	210.17	14.64	2.75
5.4	3	181.94	0	315.30	0.078	110.49	358.72	0.052	4.76
1.65	6	208.48	204.17	251.12	−0.53	36.18	83.50	13.26	0.49
2.64	6	196.45	148.19	343.56	−0.060	41.17	122.19	13.13	1.04
3.3	6	189.55	123.93	373.89	0.058	59.86	154.99	5.07	1.76
3.96	6	181.76	103.98	379.98	0.10	67.43	197.04	2.20	2.71
5.4	6	159.90	61.65	217.32	0.090	119.13	353.97	0.43	4.61

Figure 11 presents the head H and efficiency η for $M2$, $M3$, and $M6$ under the five flow conditions (Q = 1.65, 2.94, 3.3, 3.96, 5.4 m^3/h). As shown in Figure 11 and Table 8, the head and efficiency under the five flow conditions all decrease after the volumetric and interstage leakages are considered, and the decrease rate caused by the volumetric leakage is noticeably faster than that caused by the interstage leakage. These results indicate that the loss of volumetric leakage loss is greater than that of the interstage leakage. With an increase in flow rate, the decrease rates of the head and efficiency caused by the interstage leakage initially increase, subsequently decrease, and finally approach zero. By contrast, the decrease rates caused by volumetric leakage constantly decrease.

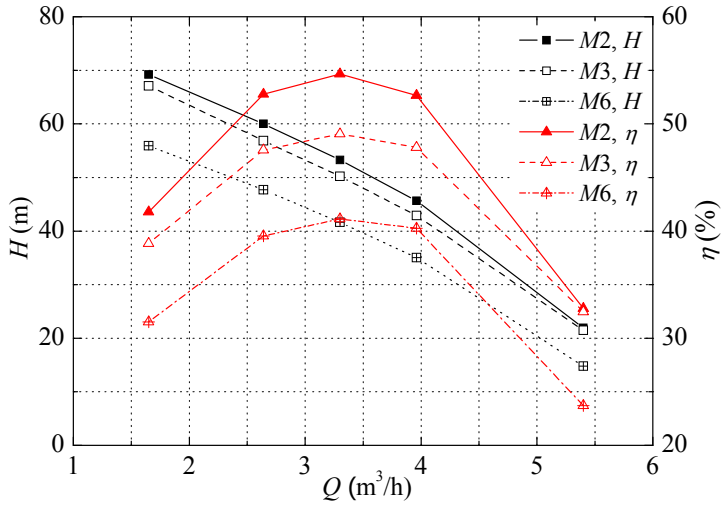

Fig. 11 Head and efficiency of three calculation models under different flow conditions

The mechanical efficiency η_m, hydraulic efficiency η_h, and volumetric efficiency η_v for *M*2, *M*3, and *M*6 under the five flow conditions are shown in Figure 12. As shown in Figure 12 and Table 9, the volumetric efficiencies for *M*2 and *M*3 are both 100% without volumetric leakage. With the increase of the flow rate and the decrease in the pressure difference between the two sides of the front ring, the volumetric efficiency for *M*6 increases from 65.29% to 91.86%, indicating that the influence of the flow rate on volumetric efficiency is extremely significant. Moreover, the mechanical efficiencies for *M*2 and *M*6 are nearly the same, but that for *M*3 is relatively low. This outcome indicates that the volumetric and interstage leakages respectively have nearly the same positive and negative correlations with mechanical efficiency. With the increase of the flow rate, the mechanical efficiencies of three models all increase, and the increase rate for *M*3 is the fastest. Under large flow conditions, the mechanical efficiencies of the three models are basically the same, indicating that the interstage and volumetric leakages have minimal impact on mechanical efficiency. In addition, both the interstage and volumetric leakages lead to the decrease of hydraulic efficiency and a shift in the highest hydraulic efficiency points of the three models to the small flow direction. With the increase of flow rate, the decrease rate of the hydraulic efficiency caused by the interstage leakage initially increases and subsequently decreases, whereas that caused by the volumetric leakage constantly increases.

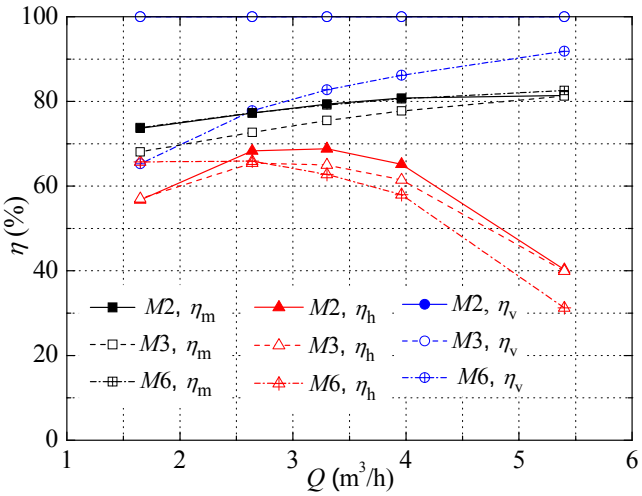

Fig. 12 Three component efficiencies for *M*2, *M*3, and *M*6 under different flow conditions

Figure 13 shows the components of the shaft power for *M*2, *M*3, and *M*6 under the five flow conditions. A comparison of Figure 13(a) and 13(b) shows that the loss of disk friction power increases after the interstage leakage is considered. The interstage leakage gradually decreases to zero with the increase of flow rate, resulting in the decline of the increase rate of the loss of disk friction power to zero; this outcome shows that a portion of the energy loss from the interstage leakage is converted by the loss of disk friction power. In addition, the hydraulic loss power of the impeller and that of the diffuser decrease, whereas that of the pump cavity increases after considering the interstage leakage. However, with the increase of flow rate, the sum of the three types of hydraulic losses decreases, and the decrease rate reduces gradually to zero. This result indicates that the remaining energy loss from the interstage leakage is also converted by the hydraulic power loss. Moreover, the working power decreases after considering the interstage leakage, and the decrease rate initially increases and subsequently reduces to approximately zero with an increase of flow rate.

A comparison of Figures 13(b) and 13(c) reveals that the loss of disk friction power decreases after the volumetric leakage is considered, and the decrease rate reduces gradually because of the decreasing volumetric leakage with the increase of flow rate. This outcome indicates that the increasing volumetric leakage decreases the loss of disk friction power. Moreover, the actual flow through the impeller increases

after the volumetric leakage is considered; as a result, the hydraulic power loss of the impeller and that of the diffuser initially decrease and subsequently increase, and the hydraulic power loss of the pump cavity decreases gradually. Additionally, the working power also decreases after the volumetric leakage is considered, and the decrease rate increases gradually with the increase of flow rate. These results show that with the increase of flow rate, the influences of the interstage and volumetric leakages on the components of the shaft power gradually weaken and approach zero under a large flow condition.

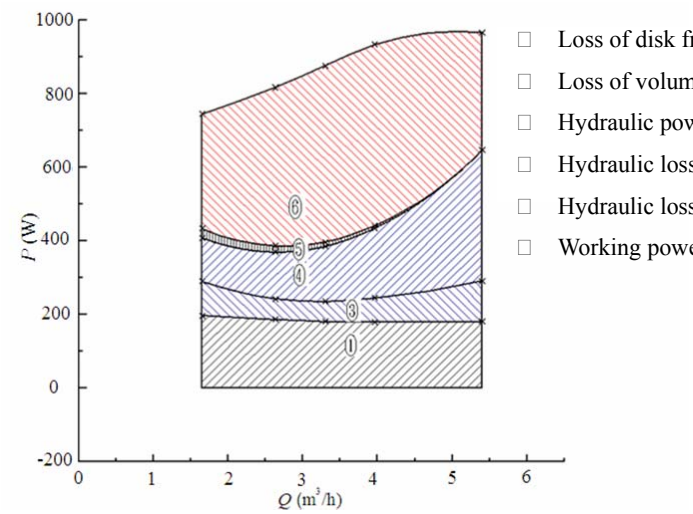

(a) *M*2

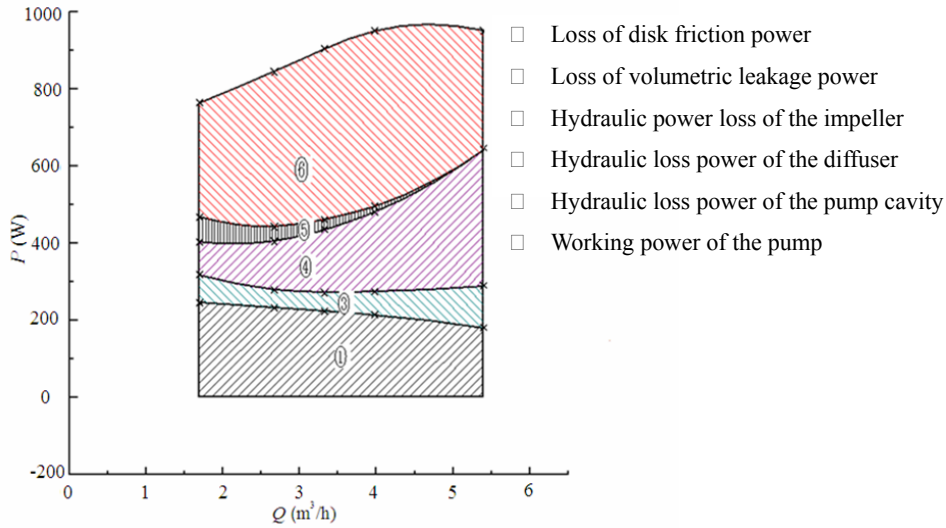

(b) *M*3

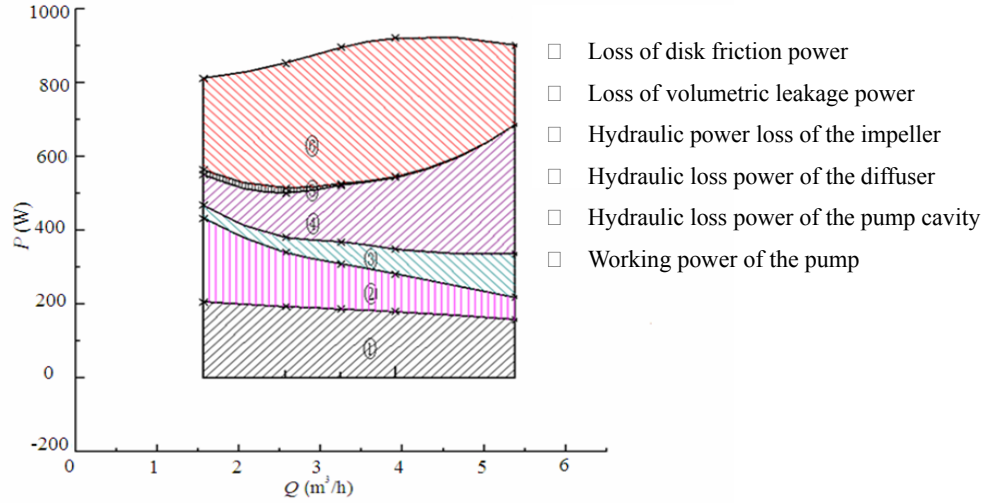

(c) *M*6

Fig. 13 Components of the shaft power for *M*2, *M*3, and *M*6 under different flow conditions

3.4 Pareto charts of shaft power's components for three typical calculation models

The Pareto charts are very useful and beautiful, using which readers can understand rapidly the interactional relationships of each factor. As this manuscript focuses on the interactional relationships among the different kinds of energy loss in the pump, Pareto charts of shaft power's components for different calculation models (*M*2, *M*3 and *M*6) under rated flow condition of Q = 3.3 m^3/h are shown in Figure 14, and those for the calculation model *M*6 under different flow conditions (Q = 1.65, 3.3 and 5.4 m^3/h) are shown Figure 15.

As can be seen in Figure 14, three typical calculation models, which respectively consider the disk friction loss, interstage leakage loss of rear ring and volumetric leakage loss of front ring, are selected as the research object for the energy loss model. For *M*2, after considering the disk friction loss, the shaft power's components are in the following descending order of magnitude: the working power (P_u), the loss of disk friction power (P_m), the hydraulic loss power of the diffuser (P_{df}), the hydraulic loss power of the impeller (P_{ip}) and the hydraulic loss power of the pump cavity (P_{ca}). Additionally, P_m accounts for 20.6% of the total shaft power, indicating that it is necessary to include the disk friction loss for the calculation model. Moreover, P_{ip} and P_{df} respectively account for 17% and 6.2% of the total shaft power, which indicates

the hydraulic performance of the diffuser is rather bad compared with the impeller. For *M*3 when the interstage leakage is considered, the order of magnitude does not change, but P_m increases sharply, while P_{df} and P_{ca} increase slightly due to the interstage backflow from the diffuser to the pump cavity. For *M*6, after considering the front ring leakage, the loss of volumetric leakage power (P_v) increases from 0 to 13.7% of the total shaft power rapidly, indicating that the leakage from the front ring is really volumetric leakage. However, the proportions of main energy losses such as the loss of friction disk power and the hydraulic loss power are almost the same as that for *M*2, implying that the influences of the front ring leakage and rear ring leakage on the main energy losses are just the reverse. Finally, with increasing integrity of calculation model, the working power continues to decrease, while the loss of friction disk power and the hydraulic loss power swings back and forth.

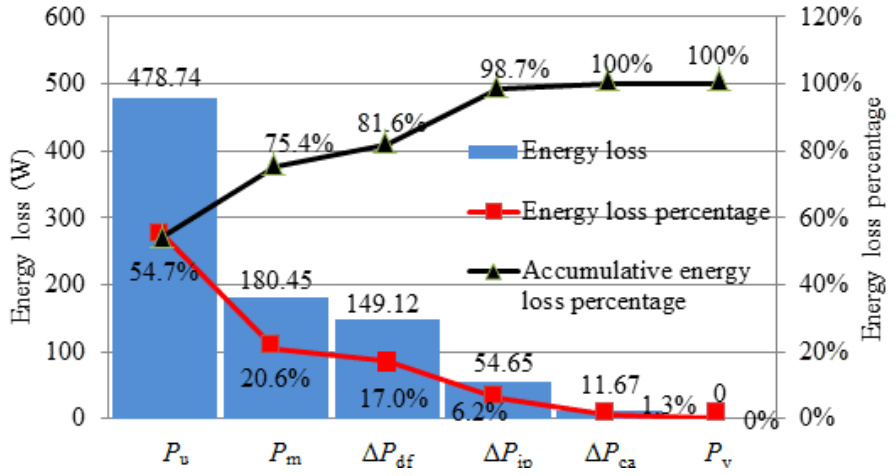

(a) *M*2

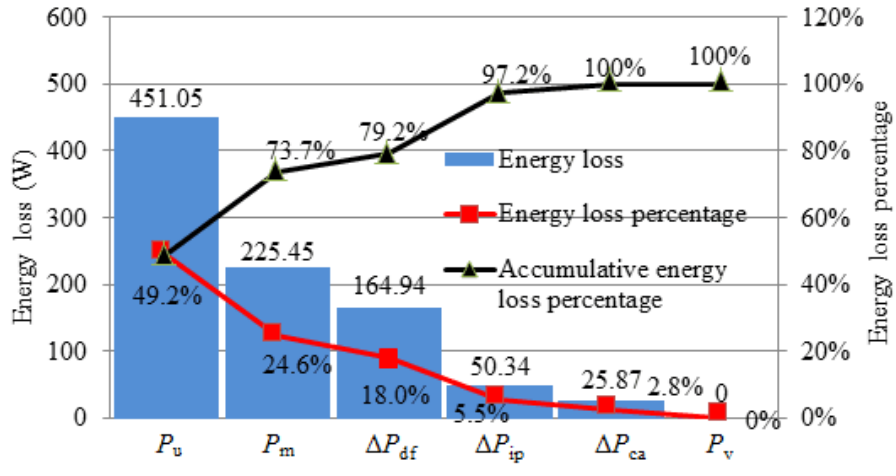

(b) *M*3

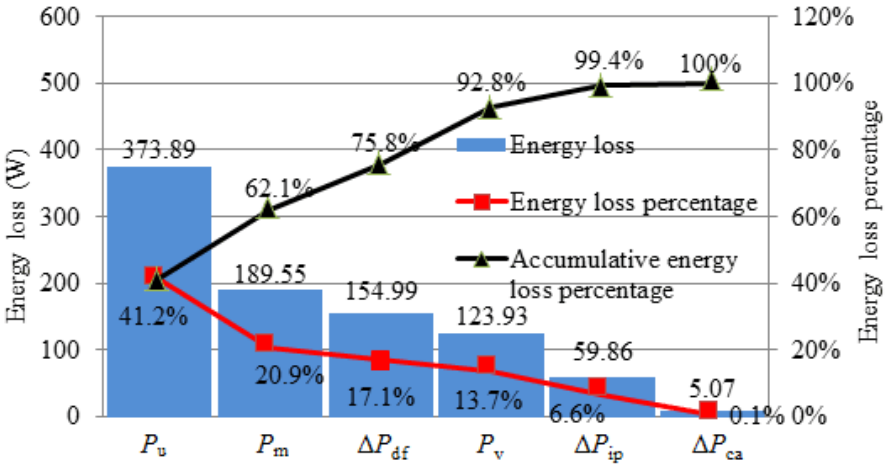

(c) *M*6

Fig. 14 Pareto charts of shaft power's components for different calculation models under rated flow condition of Q = 3.3 m^3/h

As can be seen in Figure 15, the working power accounts for a small proportion of the shaft power, indicating the large total energy loss in the pump. With the increase of flow rate, the loss of disk friction power decreases; the hydraulic loss power of the impeller initially decreases and subsequently increases; the hydraulic power loss of the diffuser increases gradually; the hydraulic loss power of the pump cavity gradually decreases to zero; and the working power initially increases and subsequently decreases until it finally reaches a maximum value near the rated flow condition (Q = 3.3 m^3/h). In a word, with the change of flow rate, each individual shaft power's component is always varying, which indicates that energy loss proportion is rather sensitive to Reynolds number.

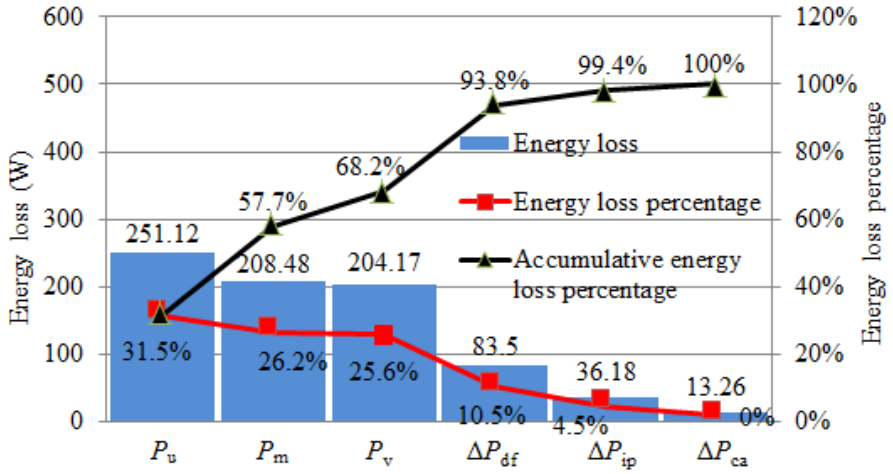

(a) Q = 1.65 m^3/h

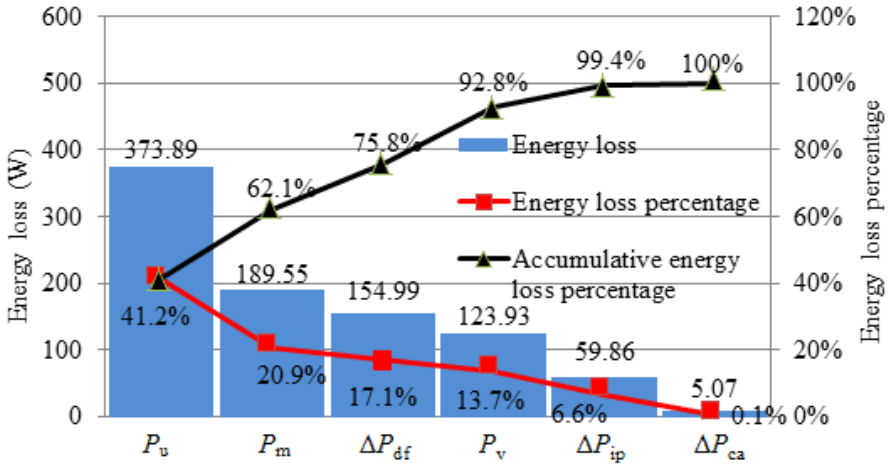

(b) Q = 3.3 m^3/h

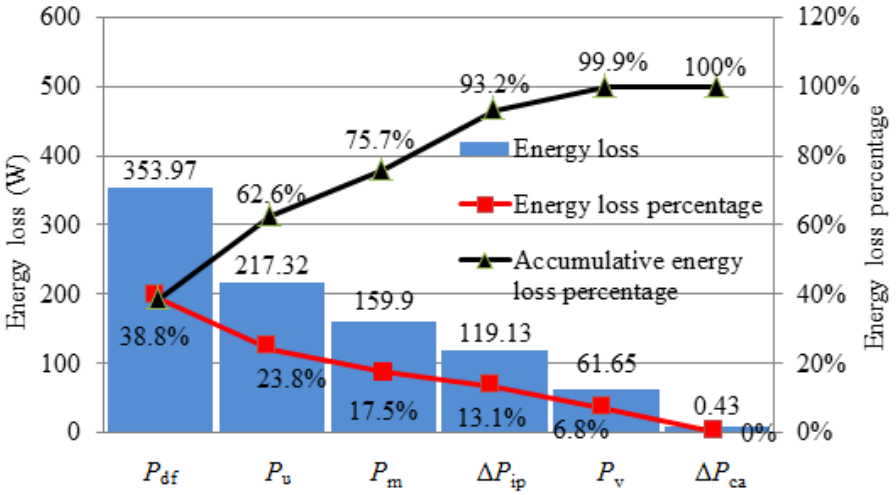

(c) Q = 5.4 m^3/h

Fig. 15 Pareto charts of shaft power's components for *M*6 under different flow conditions

3.6 Relationships between the leakage amount and energy loss power

Figure 16 shows the relationships between the leakage amount and the loss of disk friction power under the conditions where the interstage or volumetric leakage is considered or not. With the increase of flow rate, the amounts of interstage and volumetric leakages reduce continuously, and the interstage leakage is approximately zero under a large flow condition. The loss of disk friction power decreases with an increasing flow rate, but the decrease rate is considerably slow and essentially remains stable under the large flow condition for *M*2 without the interstage and volumetric leakages. The loss of disk friction power for *M*3 interstage leakage increases significantly compared with that of *M*2, and the increase rate reduces constantly with

the increase of flow rate. The loss of disk friction power decreases sharply for *M*6 with volumetric leakage compared with that of *M*3.

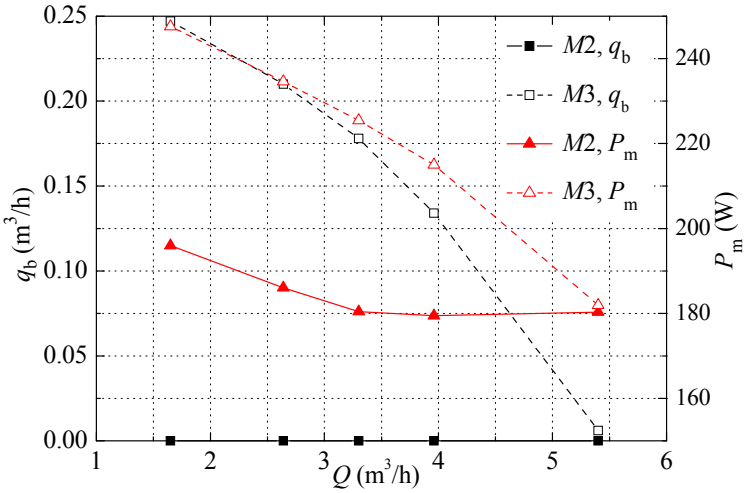

(a) With and without the interstage leakage

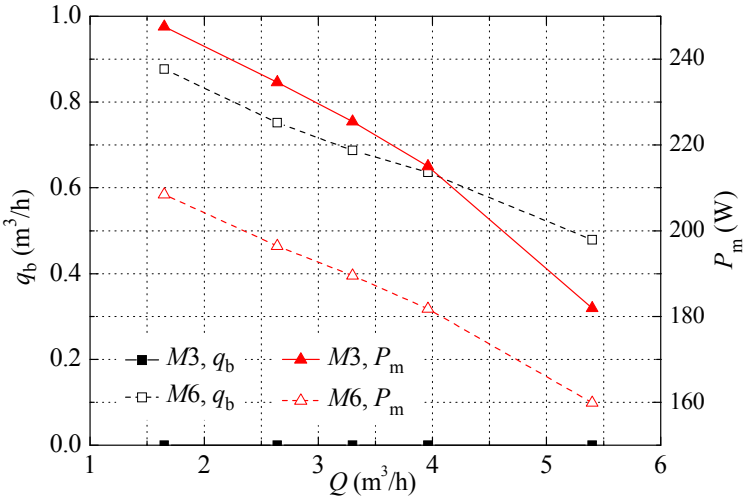

(b) With or without volumetric leakage

Fig. 16 Relationships between the leakage amount and loss of disk friction power

Assume $\Delta\zeta_1 = \dfrac{P_{M3} - P_{M2}}{P_m}$, $\Delta\gamma_1 = \dfrac{q_b}{Q_r}$, $\Delta\zeta_2 = \dfrac{P_{M3} - P_{M6}}{P_m}$, and $\Delta\gamma_2 = \dfrac{q}{Q_r}$,

where $\Delta\zeta_1$ is the increasing coefficient of the loss of disk friction power with interstage leakage, $\Delta\zeta_2$ is the decreasing coefficient of the loss of disk friction power with volumetric leakage, $\Delta\gamma_1$ is the leakage coefficient with interstage leakage, $\Delta\gamma_2$ is the leakage coefficient with volumetric leakage, P_{M2} is the loss of disk friction power of *M*2, P_{M3} is the loss of disk friction power of *M*3, P_{M6} is the loss of disk friction power of *M*6, P_m (= 180.454 W) is the reference for the loss of disk friction power

(i.e., that for *M*2 under rated flow condition), and Q_r (= 3.3 m^3/h) is the reference flow under a rated condition.

Figure 17 presents the variations of the loss of disk friction power $\Delta\zeta$ with leakage coefficient $\Delta\gamma$. The following relationships can be obtained using quadratic curve fitting:

$$\Delta\zeta_1 = -0.00316 + 6.398\Delta\gamma_1 - 33.549\Delta\gamma_1^2 \quad (18)$$

$$\Delta\zeta_2 = -0.280 + 3.851\Delta\gamma_2 - 7.450\Delta\gamma_2^2 \quad (19)$$

Both interstage and volumetric leakages exert vital influences on the loss of disk friction power. When $\Delta\gamma_1$ is approximately 0.08, $\Delta\zeta_1$ approaches 0.3. When $\Delta\gamma_2$ is approximately 0.2, $\Delta\zeta_2$ approaches 0.2. These results indicate that the interstage leakage has a more significant effect on the loss of disk friction power than the volumetric leakage has. Moreover, the changing coefficient of the loss of disk friction power increases with the leakage coefficient, but the increase rate gradually decelerates.

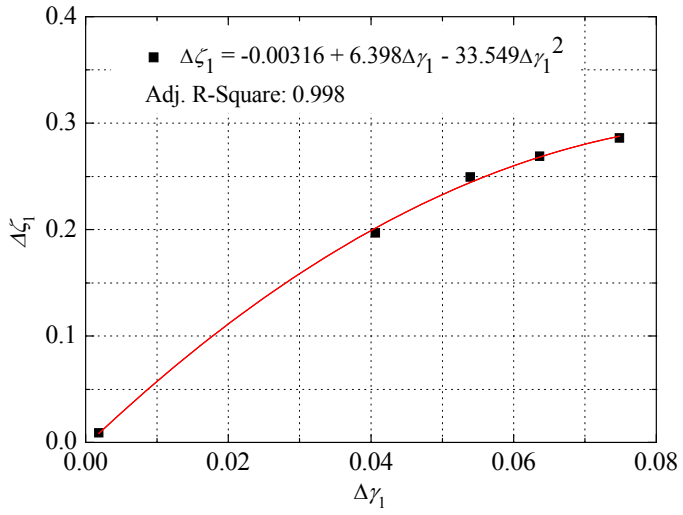

(a) Increasing coefficient of the loss of disk friction power with interstage leakage

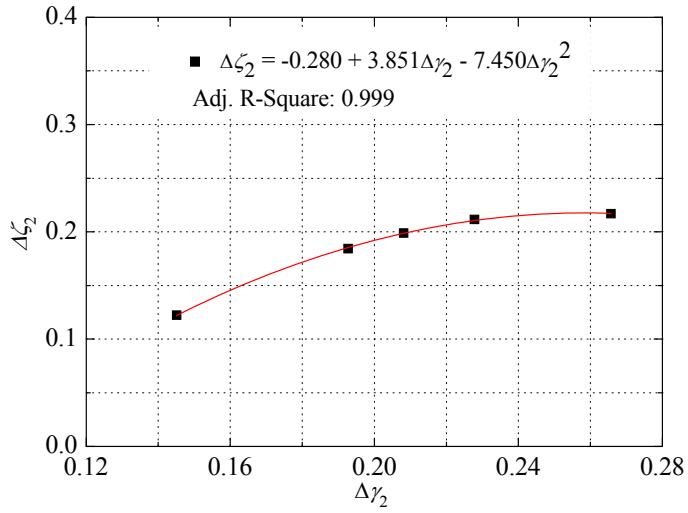

(b) Decreasing coefficient of the loss of disk friction power with volumetric leakage

Fig. 17 Relationship between the coefficients of disk friction loss and leakage

Figure 18 presents the shear stresses τ at different radii ratio r/R ($R = 0.5D_2$) of any locations on the front shroud for *M*3, *M*4, *M*5, and *M*6, which have different amounts of volumetric leakage, investigating further the relationship between the leakage amount and disk friction loss. As shown in Figure 18, the shear stress on the front shroud of the second-stage impeller is slightly larger than that of the first-stage impeller, but their overall trends are nearly the same. The shear stress on the front shroud increases linearly with the increase of radius for *M*3 with volumetric leakage. As the radii increase, the shear stresses on the front shrouds initially decrease, subsequently increase, and finally approach zero at $r/R \approx 0.5$ for *M*4, *M*5, and *M*6 with volumetric leakage. With the increase in the amount of volumetric leakage, the shear stress on the front shroud decreases gradually at $r/R > 0.5$, especially for *M*3 and *M*4.

Figure 19 shows the shear stresses at different radii ratio of any locations on the rear hub for *M*2 and *M*3, which have different amounts of interstage leakage. As shown in Figure 19, the shear stresses on the rear hub of the two impellers are almost the same. Once considered the interstage leakage, the shear stress on the rear hub increases rapidly. These results indicate that the increase of the shear stress on the front shroud is caused by the volumetric leakage, whereas the decrease of the shear stress on the rear hub is ascribed to the interstage leakage. Thus, these two types of leakages have opposite effects on the loss of disk friction power.

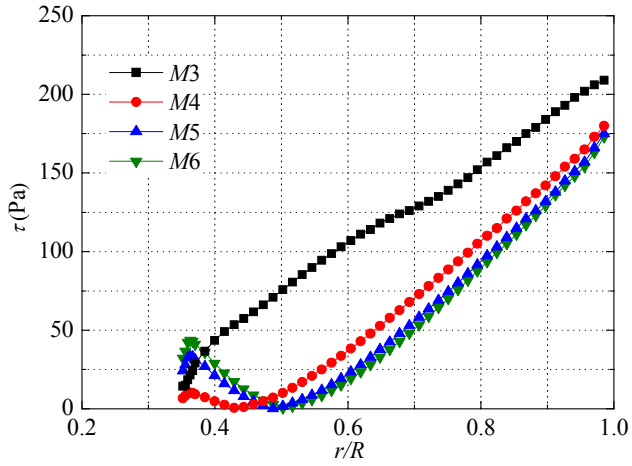

(a) Front shroud of the first-stage impeller

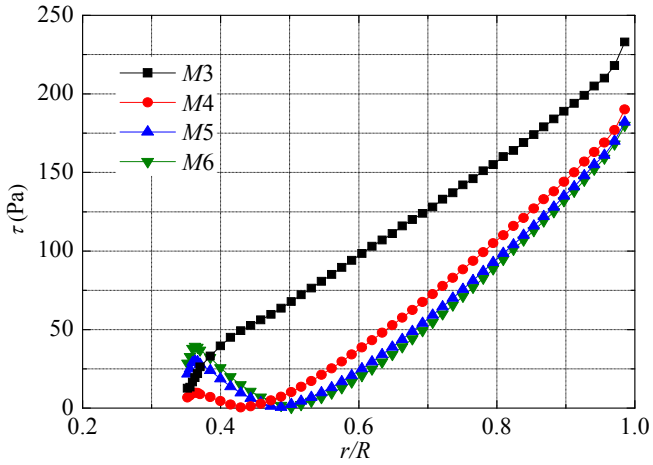

(b) Front shroud of the second-stage impeller

Fig. 18 Shear stresses on the front shroud with different amounts of volumetric leakage

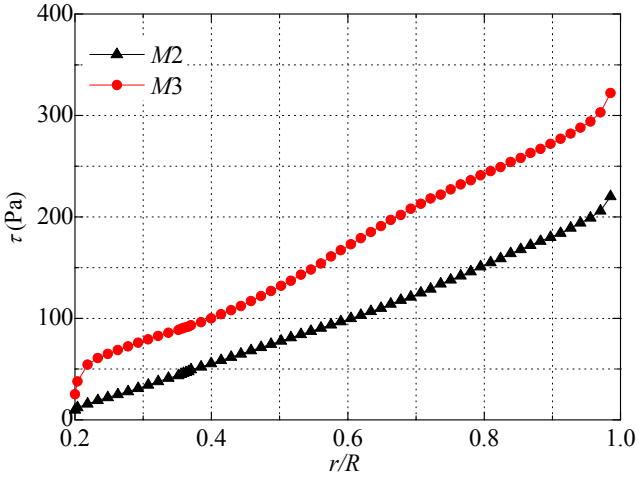

(a) Rear hub of the first-stage impeller

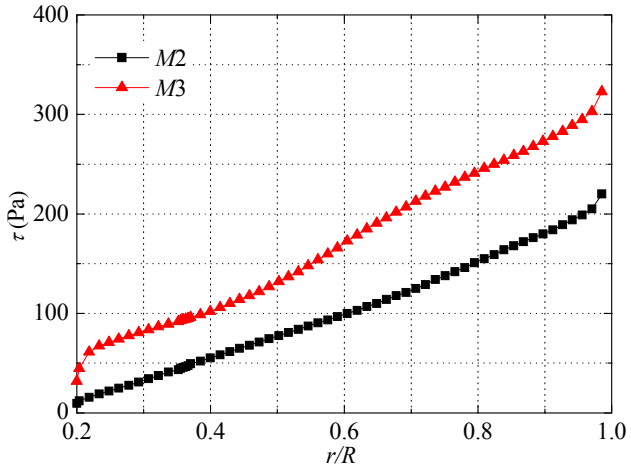

(b) Rear hub of the second-stage impeller

Fig.19 Shear stresses on the rear hub with different amounts of interstage leakage

The loss of disk friction power accounts for a small proportion of the shaft power, and the hydraulic power loss reaches the minimum value under a rated flow condition for general centrifugal pumps. With the increase of the volumetric leakage, the loss of disk friction power reduces slightly, whereas that of the hydraulic power increases sharply under a rated flow condition (actual flow shifted to a large flow condition); thus, the overall power loss remarkably increases. Therefore, the pump efficiency is reduced by increasing the gap at the front ring.

However, the loss of disk friction power for centrifugal pumps with significantly low specific speed accounts for a huge proportion of the shaft power, and these pumps are generally designed using the maximum flow design method. Consequently, the supposed rated flow condition is actually a small flow condition. With the increase of volumetric leakage, the loss of disk friction power is considerably reduced, and the hydraulic power loss also decreases rapidly under a rated flow condition (actual flow shifted to the rated flow condition). By contrast, the loss of volumetric leakage power increases significantly. However, the overall power loss may be reduced because of the interactions of the three types of energy losses, that is, the efficiency of a centrifugal pump with a significantly low specific speed under a rated flow condition may be enhanced by increasing the amount of volumetric leakage. Kurokawa conducted the following tests on a centrifugal pump with a significantly low specific speed. Cutting off a hole with a diameter of 5 mm on the front shroud was found to

increase the efficiency of the pump by 3.5%, whereas cutting another hole could decrease the efficiency to the value of the original model without any hole. The model in this study is only a centrifugal pump with a generally low specific speed. to which this law is applicable; however, the interactive relationships among the three types of energy losses cannot be ignored.

4. Optimization methods for pump efficiency

The pump efficiency can be improved by reducing the energy losses in the pump, namely, disk friction, volumetric leakage, and hydraulic losses. The disk friction loss is affected by two factors. The first factor includes the geometric parameters, such as disk diameter, rotating speed, and surface roughness, whereas the second factor includes the interstage and volumetric leakages. The disk diameter, rotating speed, and surface roughness are positively correlated with disk friction loss. The disk diameter and rotating speed are not allowed to reduce because of the high-head requirement, and the surface roughness has basically reached the theoretical minimum value. Therefore, reducing the disk friction loss by decreasing the parameters is challenging. Meanwhile, the interstage and volumetric leakages respectively show positive and negative correlations with disk friction power loss; thus, the loss of disk friction power can be decreased by reducing the amount of interstage leakage and increasing that of the volumetric leakage. However, an increase in the amount of volumetric leakage also leads to a remarkable increase in volumetric leakage loss. The increment of the volumetric leakage loss is usually greater than the decrement of the disk friction loss for general centrifugal pumps. Therefore, the total energy loss can be decreased by reducing the volumetric leakage loss, resulting in an improved pump efficiency, as shown in this paper.

As shown in Figure 13, the hydraulic loss power of the diffuser increases significantly with the increase of flow rate, implying that the carrying capacity of the diffuser is insufficient, and the size of the diffuser should be increased. Moreover, the pump in this study has a cantilever structure, and only one rolling bearing exists in the connective part between the pump and motor; thus, a large runout of the shaft may

ensue. For this reason, the clearances of the ring have to be maintained between 0.5 mm and 1 mm, as shown in Figure 20(a). Therefore, the pump efficiency can be improved effectively by the following three methods:

(1) A plastic seal ring may be placed on the front ring of the impeller, as shown in Figure 20(b). The seal ring is close to the cavity wall during pump operation, and the volumetric leakage is prevented effectively because of the pressure difference. However, this method is inapplicable for the interstage leakage because the pressure difference reduces the gap between the seal ring and the rear hub of the impeller.

(2) A sliding bearing may be installed on the inlet of the pump, as shown in Figure 20(c). The runout of the shaft decreases rapidly because both its ends are fixed, and the clearances of the front and rear rings can be set within 0.2 mm to improve the pump efficiency remarkably. However, the pump will inevitably vibrate during the operation if this method is applied.

(3) The radial dimension of the positive diffuser may be increased, as shown in Figure 20(d). A high head ($H_{max} \geq 13$ m) and a small shaft power ($P_{max} \leq 200$ W) are both required by users; thus, a small angle of the impeller outlet and a large impeller diameter have to be selected. Moreover, the unilateral radial dimension of the positive diffuser is only 4.5 mm because of the limitation of the pump diameter ($D_{max} \leq 118$ mm), resulting in an insufficient carrying capacity of the diffuser. With the increase of flow rate, the hydraulic loss of the diffuser increases significantly. Therefore, two techniques are proposed to solve these problems: removing the restrictions on either the high head or the pump diameter. The first technique can increase the radial dimension of the positive diffuser by reducing the impeller diameter. This technique can decrease not only the friction disk loss at the impeller but also the hydraulic loss at the diffuser. The second technique can increase the radial dimension of the positive diffuser directly by increasing the pump diameter.

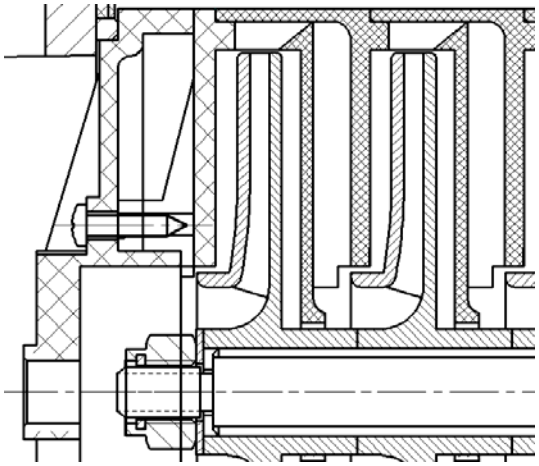

(a) Original pump model

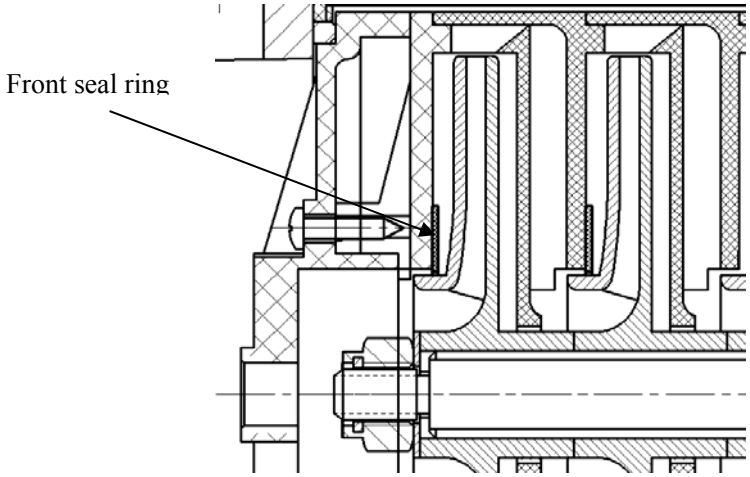

(b) Pump model with front seal ring

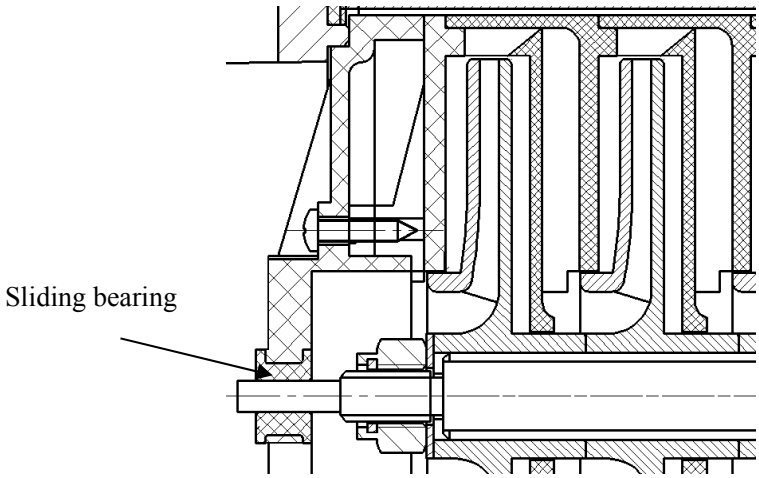

(c) Pump model with sliding bearing

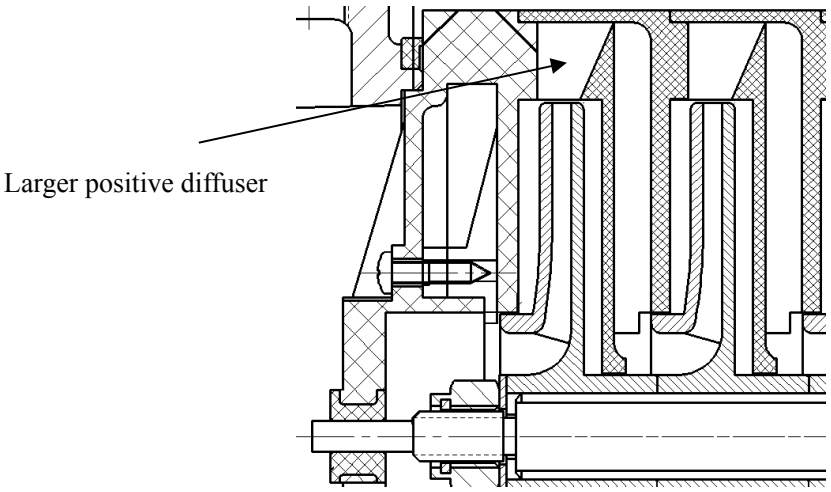

(d) Pump model with a positive diffuser with larger radial dimension

Fig. 20 Two-dimensional drawings of the proposed methods to improve pump efficiency

Due to that the plastic seal ring on the front ring of the impeller always moves slightly in the working operation of the pump, it's very difficult to make accurate calculation. Therefore, the authors decided to conduct some experiments to verify the theoretical optimal pump models. Note that only the first and the second optimal methods are used, because the third optimal method by increasing the radial dimension of the positive diffuser has not been tried due to the great change of the pump's structure and the limitation of the manuscript's revision time.

The original pump model with the front ring of 1 mm unilateral clearance is selected as model 1 (referred to as *m*1). Moreover, model 2 (referred to as *m*2) is also selected through placing a plastic seal ring on the front ring of *m*1, and the volumetric leakage is prevented effectively because of the pressure difference due to that the seal ring is close to the cavity wall during pump operation. The theoretical clearance of the front ring of *m*2 is 0.5 mm, while the actual clearance of the front ring should be larger due to the slight movement of the seal ring in the working operation of the pump. Additionally, it's not very necessary to place the sliding bearing on the inlet of the pump if only some performance experiments with short-time operation are done. Therefore, through adjusting the radial dimension of the front ring, the optimal pump model with the front ring of 0.5 mm unilateral clearances is also selected as model 3 (referred to as m3). The efficiency and the head of the three pump models are also shown in Figure 21. As can be seen that, compared with *m*1 and *m*3, with decreasing

the clearance of the front ring, the head and the efficiency under different flow conditions all decrease, and the maximum efficiency point shifts to the small flow rate condition due to the decrease of the volumetric leakage. What's more, compared with *m*1 and *m*2, the head and the efficiency of the pump are improved indeed through placing a plastic seal ring on the front ring, but the improvement of the pump performance is slightly smaller than that through decreasing directly the clearance of the front ring compared with *m*2 and *m*3. Therefore, the theoretical optimal pump models are verified through the experimental methods.

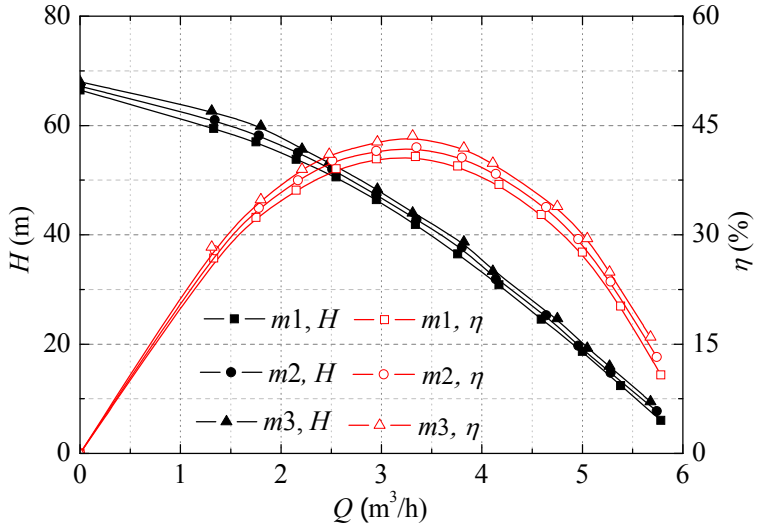

Fig. 21 Experimental results of three kinds of pump models

5. Conclusions

In this study, a combined energy loss model and Computational Fluid Dynamics (ELM/CFD) optimization method was proposed, and has been applied successfully to the design of a multistage centrifugal pump. Four different calculation models were established to systematically study the various kinds of energy losses in the pump. A series of numerical calculations were performed with different grid numbers, turbulence models, convergence precisions and surface roughness, to find the appropriate numerical settings and ensure the reliability of the results. Then, all the kinds of energy losses in a typical multistage centrifugal pump are calculated to assess their individual or combined effects on the pump performance. Finally, the optimal design were obtained by the combined method of ELS/CFD and verified by prototype

test. The analysis of the results enables the following observations to be drawn:

(1) Suitable setting methods of numerical calculation for multistage centrifugal pump could render the numerical results more credible, and the integrity of the calculation domain is the key contributor to the accuracy of CFD results. When the integrity of the calculation domain increases, the efficiency constantly decreases, and the largest deviation exceeds 50%; the head initially increases and subsequently decreases, with the largest deviation being approximately 30%. According to the detailed comparisons, the numerical and experimental results are almost coincident under rated flow condition, but there are some minor discrepancies (within 3%) under non-rated flow conditions because of flow separation or recirculation in the pump. Therefore, it is rather creditable to predict the performances of multistage centrifugal pump using CFD based on the whole calculation model and appropriate numerical setting methods.

(2) An ELM/CFD method was established for the optimal design, which includes the various kinds of energy loss in the pump, such as disk friction loss, volumetric leakage loss, interstage leakage loss as well as the hydraulic loss, which occurred at inlet section, outlet section, impeller, diffuser and pump cavity, respectively. The energy distribution in any pump models could be displayed clearly, and the abnormal energy loss could be obtained for further improvement of pump performance. For example, the hydraulic loss power of the diffuser accounts for 17% of the total shaft power, which indicates that the hydraulic performance of the diffuser is rather poor. Through the analysis found that the radial dimension of the positive diffuser is too small and large impact energy loss exists on the inlet of the positive diffuser. Therefore, the problem of low efficiency can be solved by increasing the radial dimension of the positive diffuser.

(3) The interstage leakage loss is converted by the disk friction loss, while the volumetric leakage loss is negatively correlated with the disk friction loss. The increment of the volumetric leakage loss is greater than the decrement of the disk friction loss for general centrifugal pumps. Therefore, reducing the volumetric leakage and interstage leakage losses is the most effective technique to increase the

efficiency of general centrifugal pumps. Under the premise of ensuring the working reliability of the pump, the clearance of front and rear ring should be as small as possible. Additionally, due to that the loss of disk friction power accounts for large proportion of the total shaft power of the centrifugal pump, especially the low specific centrifugal pump, so polishing the impeller shroud and pump cavity is beneficial in improving pump efficiency and reducing pump shaft power under the premise that the surface roughness has a significant influence on the pump performance.

Acknowledgments

Funding support from the Priority Academic Program Development of Jiangsu Higher Education Institutions (PAPD) and the China Scholar Council (2014083201656) are gratefully acknowledged.

References

[1] Shankar VK, Umashankar S, Paramasivam S, Hanigovszki N. A comprehensive review on energy efficiency enhancement initiatives in centrifugal pumping system. Applied Energy, 2016, 181:495-513.

[2] Hergt P H. Pump research and development: past, present, and future. Journal of Fluids Engineering, 1999, 121(2): 248-253.

[3] Zhang J, Zhang HH, He YL, Tao WQ. A comprehensive review on advances and applications of industrial heat pumps based on the practices in China. Applied Energy. 2016, 178:800-25.

[4] Olszewski P. Genetic optimization and experimental verification of complex parallel pumping station with centrifugal pumps. Applied Energy, 2016, 178:527-39.

[5] Hydraulic Institute, Europump and US-DOE, 2004. Variable speed pumping: a guide to successful applications, Hydraulic Institute, New York, NY.

[6] Zhou L, Shi W D, Li W, et al. Particle Image velocimetry measurements and performance experiments in a compact return diffuser under different rotating speed. Experimental Techniques, 2016, 40:245-252.

[7] Ma X H, Feng Q, Jiang X P, et al. Numerical simulation of unsteady pressure pulsation in multistage centrifugal pump. Journal of Drainage and Irrigation Machinery Engineering, 2016, 34(1): 26-31.

[8] Kang C, Yang X, Yu X J. Inter-stage interaction and unsteady flow characteristics in multistage centrifugal pump. Journal of Drainage and Irrigation Machinery Engineering, 2015, 33(7): 566-571.

[9] Zhou L, Shi W D, Li W, et al. Numerical and experimental study of axial force and hydraulic performance in a deep-well centrifugal pump with different impeller rear

shroud radius. ASME Journal of Fluids Engineering, 2013, 135(10): 104501.
[10] Wang C, Shi W, Si Q, et al. Numerical calculation and finite element calculation on impeller of stainless steel multistage centrifugal pump. Journal of Vibroengineering, 2014, 16(4): 2063-2074.
[11] Zhou L, Shi W, Wu S. Performance optimization in a centrifugal pump impeller by orthogonal experiment and numerical simulation. Advances in Mechanical Engineering, 2013, 5: 385809.
[12] Wang C, Shi W, Zhou L, et al. Effect analysis of geometric parameters on stainless steel stamping multistage pump by experimental test and numerical calculation. Advances in Mechanical Engineering, 2013, 5: 575731.
[13] Xu Y, Tan L, Cao S, Qu W. Multiparameter and multiobjective optimal design of centrifugal pump based on orthogonal method. Proceedings of the Institution of Mechanical Engineers, Part C: Journal of Mechanical Engineering Science, 2016, 22:0954406216640303.
[14] Rong G P. Orthogonal test design and its application in the pump's research. Journal of Drainage and Irrigation Machinery, 1995, 13(1): 27-30.
[15] Stepanoff A J. Centrifugal and axial flow pumps. New York: John Wiley, 1957.
[16] Lobanoff V S, Ross R R. Centrifugal pumps: design & applications. 2nd ed. Houston: Gulf Publishing Company.
[17] Korakianitis T, Hamakhan IA, Rezaienia MA, et al. Design of high-efficiency turbomachinery blades for energy conversion devices with the three-dimensional prescribed surface curvature distribution blade design (CIRCLE) method. Applied Energy, 2012, 89(1):215-27.
[18] Ouchbel T, Zouggar S, Elhafyani M L, et al. Power maximization of an asynchronous wind turbine with a variable speed feeding a centrifugal pump. Energy Conversion and Management, 2014, 78: 976-984.
[19] Goto A, Nohmi M, Sakurai T, et al. Hydrodynamic design system for pumps based on 3-D CAD, CFD and inverse design method. ASME Journal of Fluids Engineering, 2002, 124(2): 329-335.
[20] Passrucker H, Van den Braembussche R A. Inverse design of centrifugal impellers by simultaneous modification of blade shape and meridional contour. ASME Turbo Expo 2000: Power for Land, Sea, and Air.
[21] Zhou L, Shi W, Lu W, et al. Numerical investigations and performance experiments of a deep-well centrifugal pump with different diffusers. ASME Journal of Fluids Engineering, 2012, 134(7): 071102.
[22] Stirling T E, Wilson G. A theoretically based CAD method for mixed flow pumps. Proceedings, Eighth Tech Conf. of BPMA, Cambridge, 1983.
[23] Yuan W X, Zhang K W. The performance prediction of centrifugal pump. Pump Technology, 1991, 2: 9-14.
[24] Neumann B. The interaction between geometry and performance of a centrifugal pump. Mechanical Engineering Publications, 1991.
[25] Li S H. The un-design condition and optimization of blade-pump. Beijing: China Machine Press, 2006.
[26] Zhou L, Shi W, Cao W, Yang H. CFD investigation and PIV validation of flow field in a

compact return diffuser under strong part-load conditions. Science China Technological Sciences, 2015, 58(3):405-14.

[27] Bianchi G, Cipollone R. Theoretical modeling and experimental investigations for the improvement of the mechanical efficiency in sliding vane rotary compressors. Applied Energy, 2015, 142:95-107.

Nomenclature

Symbols		q_2	ring leakage amount of the second stage pump, m^3/h
b_2	outlet width of the impeller blade	q_b	interstage leakage amount of the multistage pump, m^3/h
D_1	inlet diameter of the impeller, mm	q_b	outlet width of the impeller blade
D_2	outlet diameter of the impeller, mm	R	radii of the front shroud or rear hub, mm
D_3	inlet diameter of the positive diffuser, mm	r	radii of any locations on the front shroud or rear hub, mm
D_h	hub diameter of the impeller, mm	Z	number of the impeller blades, –
G	grid size, mm	Z_p	number of positive diffuser blades, –
H	total head of the multistage pump, m	Z_n	number of negative diffuser blades, –
H_1	head of the first stage pump, m	α_3	inlet angle of the positive diffuser blade, °
H_2	head of the second stage pump, m	α_6	outlet angle of the negative diffuser blade, °
H_t	theoretical head of the multistage pump, m	β_1	inlet angle of the impeller blade, °
H_{in}	loss head of the inlet section, m	β_2	outlet angle of the impeller blade, °
H_{out}	loss head of the outlet section, m	η	efficiency of the multistage pump, –
h	hydraulic loss head of the unit fluid through the pump, m	η_h	hydraulic efficiency of the multistage pump, –
h_{ip}	hydraulic loss head of the unit fluid through the impeller, m	η_m	mechanical efficiency of the multistage pump, –
h_{df}	hydraulic loss head of the unit fluid through the diffuser, m	η_v	volumetric efficiency of the multistage pump, –
h_{ca}	hydraulic loss head of the unit fluid through the pump cavity, m	θ_w	wrap angle of the impeller blade, °
$M1$	calculation model without pump cavity, –	μ	surface roughness, μm
$M2$	calculation model without ring, –	τ	shear stresses, Pa
$M3$	calculation model without front ring, –	ΔP_h	hydraulic loss power of the multistage pump, W
$M4$	calculation model with 0.25 mm front ring, –	ΔP_{in}	hydraulic loss power of the inlet section, W
$M5$	calculation model with 0.5 mm front ring, –	ΔP_{ip}	hydraulic loss power of the impeller, W
$M6$	calculation model with 1 mm front ring, –	ΔP_{df}	hydraulic loss power of the diffuser, W

$m1$	real pump model with 1 mm front ring, –	ΔP_{ca}	hydraulic loss power of the pump cavity, W
$m2$	real pump model through placing a plastic seal ring on the front ring of $m1$, –	ΔP_{out}	hydraulic loss power of the outlet section, W
$m3$	real pump model with 0.5 mm front ring, –	$\Delta\gamma_1$	leakage coefficient with interstage leakage, –
N	Stage number of the multistage pump, –	$\Delta\gamma_2$	leakage coefficient with volumetric leakage, –
P	shaft power of the multistage pump, W	$\Delta\zeta_1$	increasing coefficient of the loss of disk friction power with interstage leakage, –
P_1	shaft power of the first stage pump, W	$\Delta\zeta_2$	decreasing coefficient of the loss of disk friction power with volumetric leakage, –
P_2	shaft power of the second stage pump, W		
P_{1h}	hydraulic power of the first stage pump, W	*Subscripts*	
P_{2h}	hydraulic power of the second stage pump, W	ca	pump cavity
P_{1m}	loss of disk friction power of the first stage pump, W	h	hydraulic
P_{2m}	loss of disk friction power of the first second pump, W	df	diffuser
P_m	loss of disk friction power of the multistage pump, W	hb	rear hub
P_{M2}	loss of disk friction power of $M2$, W	in	Inlet section
P_{M3}	loss of disk friction power of $M3$, W	ip	impeller
P_{M6}	loss of disk friction power of $M6$, W	m	mechanical
P_h	hydraulic power of the multistage pump, W	n	negative diffuser
P_v	loss of volumetric leakage power of the multistage pump, W	out	outlet section
P_u	working power of the multistage pump, W	p	positive diffuser
Q	flow rate, m^3/h	r	rated
Q_r	rated flow, m^3/h	t	theoretical
q	average ring leakage amount of the multistage pump, m^3/h	v	volumetric
q_1	ring leakage amount of the first stage pump, m^3/h	w	wrap

1